CHALMERS

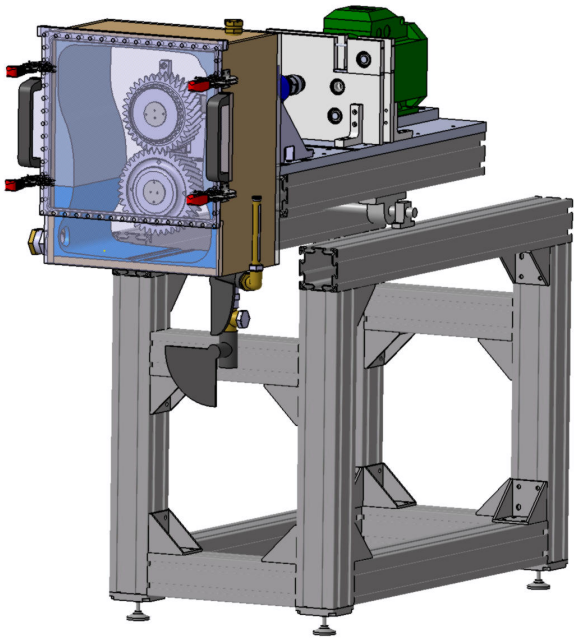

Design and evaluation of a test rig for measuring gear related losses within a Volvo Trucks gearbox

Master Thesis in Mechanical Engineering

SEBASTIAN ELIASSON
ANDRÉ FRANSSON

Department of Mechanics and Maritime Sciences
Division of Fluid Dynamics
CHALMERS UNIVERSITY OF TECHNOLOGY
Gothenburg, Sweden 2021, www.chalmers.se

Master's Thesis in Applied Mechanics 2021

Design and evaluation of a test rig for measuring gear related losses within a Volvo Trucks gearbox

Sebastian Eliasson
André Fransson

Department of Mechanics and Maritime Sciences
Division of Fluid Dynamics
Chalmers University of Technology
Gothenburg, Sweden, 2021

Design and evaluation of a test rig for measuring gear related losses
within a Volvo Trucks gearbox
Sebastian Eliasson & André Fransson

Master's Thesis 2021:28
Department of Mechanics and Maritime Sciences
Division of Fluid Dynamics
Chalmers University of Technology
SE-412 96, Gothenburg, Sweden

Design and evaluation of a test rig for measuring gear related losses within a Volvo Trucks gearbox

Master Thesis

by

Sebastian Eliasson, André Fransson

Department of Mechanics and Maritime Sciences
Division of Fluid Dynamics
Chalmers University of Technology
Gothenburg, Sweden

Abstract

With new EU regulations for CO_2 emissions from trucks coming into effect 2025 and 2030 there is need at Volvo Trucks to reduce the emissions produced by their trucks. An important part in that is the transmission where losses due to friction and churning is prevalent. This ever-continuing work in finding and reducing losses requires better and more precise test rigs. The current gearbox test rig at Volvo Group Trucks Technology is not able to isolate and measure losses with the desired accuracy.

This thesis therefore aimed at designing a new gear test rig through a collaboration between Chalmers University of Technology and Volvo Group Trucks Technology with better accuracy. Concepts were evaluated through the commonly used decision-matrix method with gradings based on available data and results from Finite Element Analyses and physical tests. Computational Fluid Dynamics simulations was then used to verify design choices.

The newly designed gear test rig can measure smaller losses, run different test configurations faster and simultaneously reduce or eliminate many of the uncertainties present in Volvo GTT's test rig. It also allows for axial visual inspection of the flow through its two transparent walls. One big difference between Volvo GTT's test rig and the new rig is that the new one only tests a gear pairing and hence isolates the losses from that pair.

Acknowledgements

We would like to thank our supervisors, Henrik Hagerman, Lars Jacobsson and Maria Petersson at Volvo GTT for providing us with an office space, computers, software and most of the equipment needed to perform this master thesis. We would also like to thank our examiner, Valery Chernoray, at Chalmers University of Technology for taking on the responsibilities that comes with this task. All of you have provided assistance regarding any doubts and have exceeded our expectations in doing so in a very efficient manner throughout the thesis. You have all shown a genuine interest in our success within the project for which we are forever grateful.

We would also like to thank our colleagues at both Volvo and Chalmers, for providing insightful guidance in the design process, as well as for providing necessary CAD files, 3D prints and purchases. This help has significantly improved the outcome of the project.

Last we would like to thank our family and friends, for supporting us in both the easy and hectic times of the project.

Contents

Nomenclature

Upper-case Roman

W	Deflection [m]
F	Force [N]
E	Elastic modulus [N/m^2]
I	Moment of inertia [kg$\cdot m^4$]
M	Torque [Nm]
A	Plate area [m^2]
C	Courant–Friedrichs–Lewy number [-]

Lower-case Roman

u_{tot}	Total standard uncertainty [W]
u_c	Combined standard uncertainty [W]
e	Distance [m]
m	Unbalanced mass [kg]
u	velocity [m/s]
u	Plate distance [m]
r	Radius [m]

Upper-case Greek

μ	Viscosity, [N$\cdot s/m^2$]
Ω	Rotational speed, [rad/s]
τ	Shear stress, [Pa]

Abbreviations

AMT	Automated manual transmission
CAD	Computer-Aided Design

CAN Controller Area Network

CFD Computational Fluid Dynamics

CFL Courant–Friedrichs–Lewy

DAQ Data Acquisition

ECU Electronic Control unit

FDM Fused Deposit Modeling

FEA Finite Element Analysis

FS Full Scale

FZG Forschungsstelle fur Zahnrader und Getriebebau

IPS Intresseföreningen För Processäkerhet

MRF Moving Reference Frame

PIV Particle image velocimetry

PMMA Poly(methyl methacrylate)

RBM Rigid Body Motion

SLS Selective laser sintering

TECU Transmission Electronic Control Unit

VOF Volume Of Fluid

Volvo GTT Volvo Group Trucks Technology

1 Introduction

A good gearbox is an integral part of a good truck, it effects both the performance, in terms of reliability and the overall user experience and driveability of the vehicle. Furthermore, the benefits of an automatic gearbox compared to a manual one are many, especially for professional drivers where the amount of work is greatly reduced. This includes the possibility to computerize a large part of Eco-driving and reduce the fuel consumption for drivers with a wide range of skills.

Today Volvo Trucks only produces trucks with automatic transmissions. For the diesel-powered trucks the state of the art 12 speed I-Shift intelligent automated manual transmission (AMT) is used. In addition, two additional gears available with the crawler gear option. The I-Shift AMT is based on a traditional unsynchronized manual transmission which has superior reliability and lower shift time compared to a synchronized counterpart. It consists of up to 6 gear pairings and a planetary gear set [1]. These 6 gear pairings are mounted on the input shaft, main shaft and counter shaft. The input and main shaft is mounted in a line while the counter shaft is mounted below these and is the one in connection with the standing oil. Figure 1 shows a whole I-Shift gearbox with a cutaway to display the gear and shaft configuration. The I-shift gearbox can also be combined with I-See to analyze and remember hills to better predict what gear to use and when to use engine breaking to reduce fuel consumption.

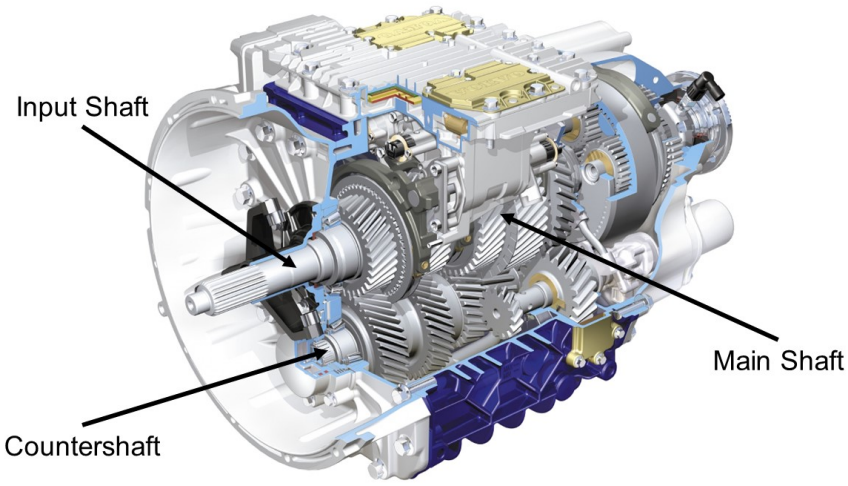

Figure 1: I-shift AMT, Image courtesy of Volvo Trucks

The fully electrical heavy-duty Volvo trucks are available with the I-shift gearbox. For the medium-duty trucks a newly introduced 2 speed gearbox is used, an image of electrical power train can be seen in figure 2.

Figure 2: Medium-duty electrical power train, Image courtesy of Volvo Trucks

Diesel powered Heavy-duty vehicles such as trucks and busses have on average an efficiency of 34% [2]. The majority of the losses are thermal losses through exhaust and cooling of the engine. The transmission frictional losses constitute on average 5.1% of the total fuel energy. Figure 3 shows a more detailed breakup of how the losses are transferred through the vehicle, marked in read is the transmission losses.

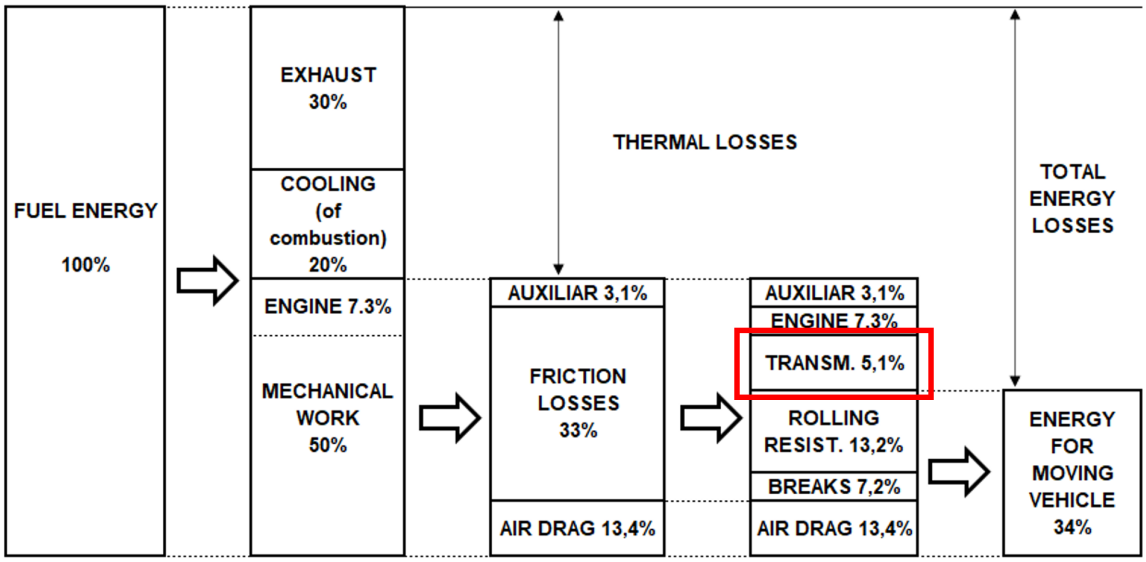

Figure 3: Energy flow in a average heavy duty vehicle [2]

Due to AB Volvo's continuous work to be a company with net-zero emissions before 2050 Volvo Group Trucks Technology (hereafter referred to as Volvo GTT) seeks to be able to identify and accurately measure as many losses as possible in as many components as possible with one of them being the gearbox [3]. The current gearbox test rig at Volvo GTT is only able to test a whole gearbox assembly which makes it hard to identify losses from separate gearbox components. A new test rig built to measure and isolate these losses are therefore needed. Particularly churning losses from individual gears and gear pairs, as well as the influence on these losses of the gear geometry, gear rotational speed, oil level, oil temperature, gearbox

housing shape, gearbox tilting angle and oil gutters. An oil gutter is a cylindrical metal plate placed under the gear to guide and control the oil flow.

1.1 Aim

The objective is to deliver a complete CAD assembly with technical drawings of a test rig of a simplified Volvo truck gearbox, which can measure losses with a precision higher than what is currently possible at Volvo [4]. This is to be completed within the twenty weeks from the start of the project.

1.2 Previous studies

There have been many previous test rigs built and many studies conducted on the subject of analysing flow between gears and measuring losses in gearboxes. In this section the rigs that will be used to assess the performance of the new rig are presented.

1.2.1 Test rig and previous studies at Volvo GTT

Earlier studies conducted at and in collaboration with Volvo GTT have only observed complete gearbox assemblies. The current Volvo GTT gearbox rig consists of an electrical motor connected to a HBM T12 torque sensor. For a fast change of test object and reduction in down time a carrier system is used where the gearbox can be prepared and mounted on the carrier while another test object is being tested in the rig. The carrier-gearbox assembly is mounted on a tiltable base to be able to simulate hilly conditions by pitch the whole test rig. The current rig does not have the ability to change roll or simulate dynamic movement. A schematic diagram of the rig can be seen in figure 4.

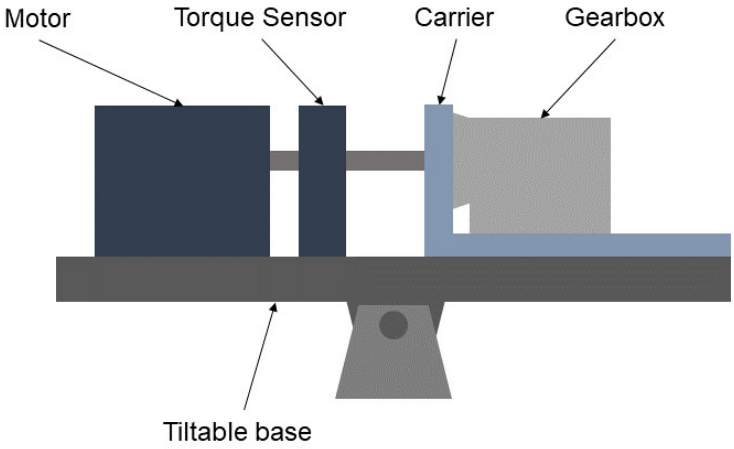

Figure 4: Schematic diagram of the Volvo gearbox test rig

To be able to reproduce the same oil temperature between different tests a portable oil conditioning rig is used which has the ability to control the temperature with a accuracy of $\pm$ 0.1 °C in steady state operation, see figure 5. The system uses the CAN standard for communication to electronic control units (ECU) and sensors.

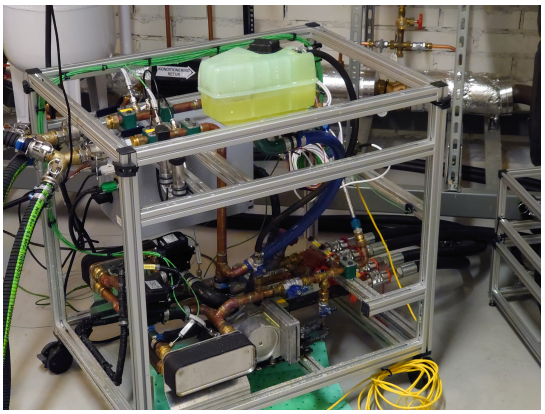

Figure 5: Oil conditioning system currently used at Volvo GTT, Image courtesy of Volvo GTT

A study conducted by Oskar Lygner [4] measured losses for different proposed transmission designs including 16 different factors. The measurements of the losses in that study had an aggregated uncertainty of 55 W at 1200 RPM which resulted in some results being inconclusive. The aggregated uncertainty consisted of uncertainty from sensors, power averaging process, due to repeatability and reproducibility with the uncertainty being 5 W, 10 W, 5 W and 15 W respectively for each source.

1.2.2 Chalmers Gear Test rig

For the development of oils and gear phenomena research, such as micro-pitting, the standardized Forschungsstelle fur Zahnrader und Getriebebau (FZG) gear test rig is commonly used all over the world [5]. Accompanying the test rig there are standardized tests for determining scuffing load-carrying capacity of oil and grease using which are described in ISO 14635-1, ISO 14635-2 and ISO 14635-3 [6][7][8]. A gear test rig based on the FZG gear test rig is currently used by Chalmers for their oil flow studies [9], a rendition of the rig can be seen in figure 6.

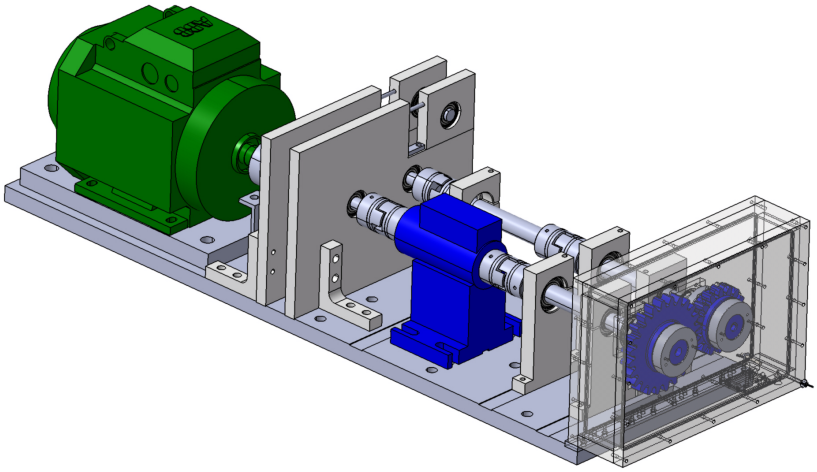

Figure 6: Chalmers gear test rig, a modified FZG gear test rig [9]

The Chalmers test rig consists of a ABB electrical motor capable of speeds up to 3000 RPM, a Kistler torque sensor (variant number: 4503A20L00B1CD1) with the performance ± 20 N·m accuracy better than 0.01% FS and a transparent PMMA box enabling particle image velocimetry (PIV) studies. The rig also have two driven shafts making it possible to run gears without meshing and just measure the torque on one gear. The rig has the capability of increasing the oil temperature through a heating pad mounted on the underside of the box. The current bearings used for both shafts are four SKF 6004-2Z bearings, two for each shaft.

A number of studies have been performed at Chalmers on this modified FZG test rig with a main focus on capturing the fluid flow using PIV [9] [10] [11].

1.2.3 Other studies

A similar study of the fluid flow with final drive gear pairs from an automotive transmission was done at the Ohio State University [12]. In this study, a in house-built rig different from the FZG gear test rig was used. The results in this study are, as the ones from Chalmers, focused on the fluid flow. It concluded that gear teeth, as compared to a smooth cylinder surface, increased losses between 30-70% when partially or fully submerged in oil.

Wind turbine gearboxes are subject to churning losses and a study conducted at the University of Porto investigated the flow in wind turbine gearboxes and the effects of different lubricants. It concluded that the transition to the turbulent flow regime occurred at a lower critical Reynolds number than suggested by the planetary gear churning loss model [13] and that a correction to this model should be done for this use case[14].

1.3 Scope

The time budget for the project is twenty weeks of full-time work for two persons, $20x40x2$ h $= 1600$ h. There is no specific funds budget for the project. Chalmers will fund the project through buying the necessary parts if they consider the cost to be reasonable.

The requirements and delimitation of the rig was divided into must, should, could and wont's. These are all given in the paragraphs below.

The rig must be able to accommodate and measure torque on one gear running at speeds up to 3000 RPM. The aggregated uncertainty must be less than 55 W at 1200 RPM. An operator must be able to empty/fill the rig with oil and be able to interchange gears in less than 4 hours. Tests must be able to be run at the installation shaft angle on flat ground, 4° incline. The rig must be able reproduce the range of viscosity the 97307 transmission oil has between $20°C-80°C$. The oil level must be able to be measured to within $\pm$ 1 mm. A visual inspection on the flow in the axial direction must be possible.

The rig should be able to support two shafts with one gear on each shaft. The incline angle should be able to deviate with $\pm 11.3°$ from the installation angle. The rig should be possible to fill/empty with oil in a matter of minutes. Furthermore, an operator should be able to change test objects in less than 2 hours. Finally, it should be possible to run tests with an oil gutter.

Additional functionalities that will be considered are the abilities to test shafts with multiple

gears up to complete main-, input and countershafts. Tilting the rig around the installation angle more than $\pm 11.3°$ will also be considered. Depending on the final concept, the oil flow in the conditioning system might be a necessary parameter to measure.

The rig will not necessarily be possible to operate from a different room. It will not be possible to test the planetary gear in the existing AMT gearbox. The distance between the shafts will be fixed. The rotational speed of the shaft driven by the motor will not go above the given 3000 RPM stated in the must-list. The rig will only be able to run tests at constant speeds between ± 3000 RPM. The pinion will rotate as freely as possible, meaning that the rig will only transfer very small torques between the gears. Finally, the rig will not be designed to accommodate for PIV studies.

The computational resources available are four personal computers and a computer cluster. Two of them with 16 GB of RAM and each running STAR-CCM+ 2020.2.1. The STAR-CCM+ licences are provided by Chalmers. Volvo has provided two computers for general use and CAD work in Catia V5. For running CFD simulations Volvo has generously provided access to their computer cluster with allocations depending on the current usage.

1.4 Societal, ethical and ecological aspects

In the EU the CO_2 emissions from heavy-duty vehicles such as lorries and busses are rising. As a result of this the EU implemented it's first CO_2 emission standard for these vehicles in 2019. Targets for average CO_2 emissions for newly produced heavy duty vehicles for 2025 and 2030 were also implemented which is expected to reduce the emissions between 2020 and 2030 by around 54 million tonnes of CO_2.

Manufacturers such as Volvo trucks will have to meet these targets, a reduction of 15% and 30% in CO_2 emissions for 2025 and 2030, respectively. Manufacturers are always actively searching for new methods to reduce emissions. One of the many parts researched and investigated by Volvo GTT is the transmission.

Since much of the losses of the transmission in a truck are present in the gearing house and the oil flow inside it, this part is of interest. Losses from the oil flow inside the gearbox increase the fuel consumption, however the churning enables the oil to lubricate and cool the components inside the gearbox. Without cooling and lubrication, the lifespan of the gearbox will be drastically reduced. Thus, it is important to find an optimum between too much churning losses and to little cooling and lubrication.

As electrification of vehicles become more common, the efficiency of the transmission becomes more vital. This is due to the fact that electric engines are a lot more efficient than combustion engines, to the extent that the efficiency of the engine is on the same level as the efficiency of the transmission. Therefore, improving the efficiency of the transmission is arguably as important as improving the efficiency of the engine.

2 Theory

In a gearbox there are losses arising from each of the different components. In this project the focus is on measuring the losses in a gear and in gear pairings. The gears in a Volvo Trucks AMT gearbox are lubricated by partially rotating in an oil bath. Furthermore the gears are suspended on rotating shafts which, in turn, are held up by bearings, see figure 7. The gears are enclosed in a gear housing. To contain the oil in the gear housing, there are seals between the housing and rotating shafts.

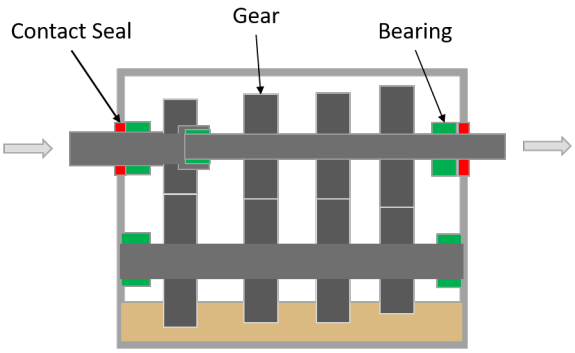

Figure 7: A schematic of a typical gearbox configuration. Arrows show component type and colors indicate same type of component

As stated, the focus is on measuring the losses in a gear and in gear pairings. The losses associated with these components are friction between the teeth, drag forces from oil and air, and squeezing of oil between the gears [11] [12] [15]. The drag force and squeezing losses are discussed in detail in this chapter.

When measuring gear pairings and its losses there are other losses and effects that impact the result in an uncontrollable way. This causes uncertainties in the results. Losses outside the gears are friction in both bearings and seals [16] as well as drag forces on the shafts [15]. The effects are aeration of oil and heat transfer from gears to oil. The effects too are discussed in detail in this chapter.

2.1 Drag force

There are two types of drag forces in a gearbox, one due to the oil and one due to the air [17]. The drag forces due to air/wind, also called windage, are prevalent on all surfaces moving through the air. Windage on gears exist in a real gearbox but windage on the shaft will affect the torque measurement and contribute to the measuring uncertainty.

The other drag force, due to the oil, is called churning. Churning follows the same logic as that for windage. It exists in a real gearbox and thus needs to be included. However, oil touching the shaft will affect the torque measurement here as well. Since oil has a much higher density than air it takes more energy to accelerate it. This makes the churning losses a lot larger than the windage losses. However, which is larger rarely matters as windage and churning are often considered together.

2.2 Squeezing of oil

The partially submerged gear pulls up oil in its pockets. As this oil comes close to the gears point of contact, it is squeezed out of the pocket on the sides of the gears. This extraction of oil requires work and will results in losses. However, oil attaching and detaching from the gears is an important part of cooling the gears.

2.3 End wall effects

The profile of the walls located radially from the gear in a gearbox can all easily be implemented in a test rig, see figure 8. The walls located axially in a gearbox is highly complex to accommodate for in a test rig. This is because in a gearbox, the gears are located very close to both each other and the walls, see figure 9. This creates very complex oil flow interactions axially, which cannot be accommodated for in a test rig without making the test rig highly complex as well. A solution is to have as little axial interference as possible on the oil flow, thereby removing its effects from the equation, see figure 9. In order to not get any interference from the axial end walls, they need to be far away enough from the gear that the tangential velocity gradient near the wall can be neglected. If this condition is not met, the walls will slow the oil flow which can affect the flow in the entire test rig. If a different test subject is then introduced, the effect could differ from the first test subject.

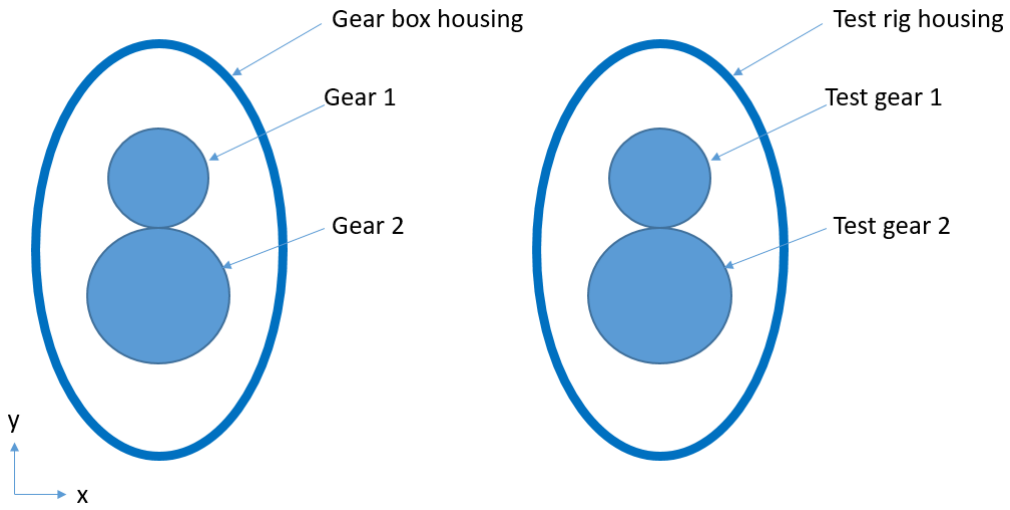

Figure 8: Radial view of a gear pair in a gearbox and in a possible test rig

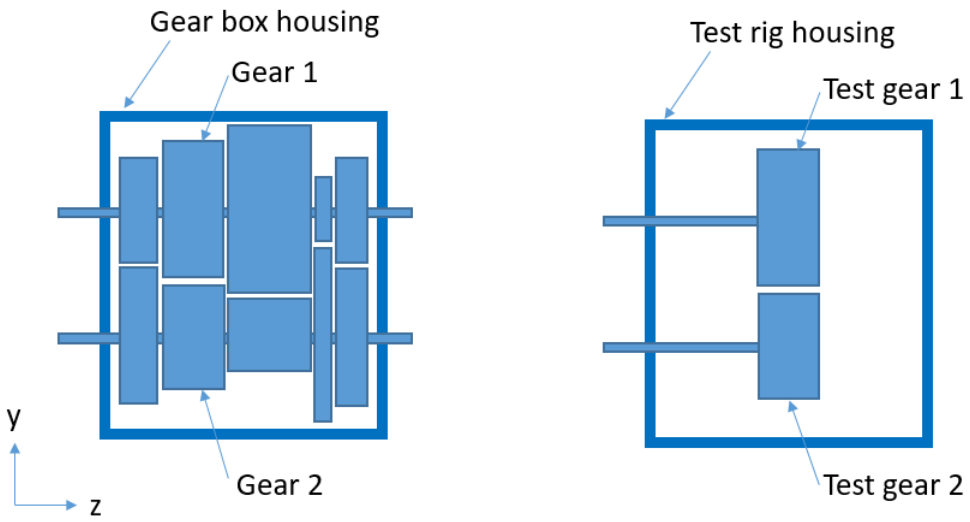

Figure 9: Axial view of gears in a gearbox and in a possible test rig

2.4 Aeration

As the gear moves through the free surface of the oil it mixes air into the oil which causes the oils properties to change. Air also gets mixed into the oil due to the oil splashing down onto the free surface. Both the viscosity and density of the fluid changes with an amount proportional to the rotational speed of the gear. The change in viscosity affects the size of the churning losses [10].

2.5 Heat sources

The churning losses and aforementioned squeezing of oil generates heat due to viscous shear in the bulk flow. Another phenomenon inside the gearbox heating the oil is the heat transfer between the gears and the oil. As mentioned in section 2 there are friction losses in the gears. The friction generates heat that is mainly transferred to the oil [16] and as the oil viscosity is highly dependent on temperature the oil flow will change with the oil temperature.

2.6 Uncertainties

Uncertainties in measurements of torque arises due to the unwanted losses and effects mentioned in 2. Other factors for uncertainty stem from repeatability, reproducibility and sensors uncertainty. These can be estimated, calculated or researched for each relevant phenomena or component of the rig. To calculate the aggregated uncertainty of a whole system the method of summation in quadrature are first used to combine the standard uncertainties, see equation 1. This method of summing is done to incorporate the error propagation.

$$u_c = \sqrt{u_1^2 + u_2^2 + u_3^2 + u_4^2 \ldots} \tag{1}$$

As two measurements both have the uncertainty u_c the error propagation that occurs when comparing two measurements has to be taken into account. Including the effects of error propagation

from two measurements the total standard uncertainty becomes.

$$u_{tot} = \sqrt{u_c^2 + u_c^2} \tag{2}$$

If one assumes that all of the measured values belong to a normal distribution using a confidence interval of 95% results in a total uncertainty of $\pm 2 * u_{tot}$.

2.7 Static forces on a shaft

The designed shafts need to be able to withstand the static forces. This is restricted by two requirements. One is a maximum radial deflection at the end of a shaft. The second is that the maximum stress in the shaft must be small enough for the shaft not to break. This is solved through a static equilibrium equation, equation 3. The deflection, W is a function of L, the length of the shaft, the radius of the shaft, the Young's modulus of the material, E, the location of the supports and the location and magnitude of the applied force, F [18]. With a set length of the shaft and a set force on the shaft, the remaining parameters can be decided. That is, the location of the supports can be decided, as well as the material and minimum diameter of the shaft.

$$W = \frac{F}{6EI}(x^3 - 3Lx^2) \tag{3}$$

2.8 Dynamic stability of a shaft

There are two requirements regarding the dynamic stability. The first is that the shaft is able to withstand the additional forces applied by rotation so that it does not break. The second is that the shaft must not self-resonate at any desired rotational speed. Otherwise, there could be large vibrations in the test rig which can affect the measurements. The possible unbalance in this case is called static unbalance, and is given by

$$F = me\Omega^2 \tag{4}$$

Figure 10 is a schematic of how the variables in equation 4 relate to the shaft.

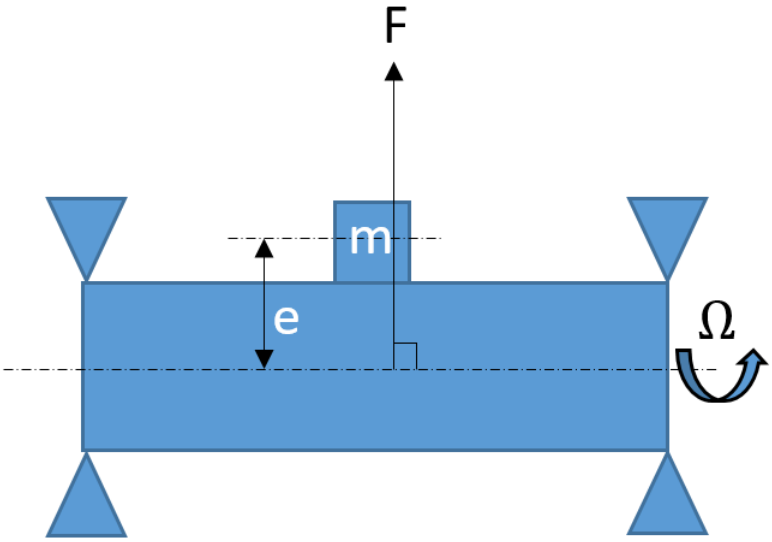

Figure 10: Static unbalance force

The force F arise from an unbalanced mass m being a distance e away from the axis of rotation. Ω is the rotational speed [19]. This unbalance force will, in contrast to the static force, change direction as the shaft rotates. Therefore, if the shaft rotates at its natural frequency, the shaft will self-resonate. Thus, the shaft must be designed so that its natural frequency is outside the range of the desired rotational speeds.

2.9 Shaft seals

Three main options are in use today for sealing shaft. These are a small radial gap, rubber seals and labyrinth seals. All of them have benefits and disadvantages depending on the application. Both the small radial gap and labyrinth seal have no contact between components and hence no direct friction losses compared to the traditional rubber seal which have lips that are in direct contact with the shaft. However, for a better seal a smaller gap and a higher mounting precision is required. The labyrinth seal also has an additional requirement for axial mounting and is also comparatively expensive compared to the two other options.

The main advantage of the rubber seal is its ability to seal when submerged at standstill whereas the non-contact ones have a gap where a small leak can happen.

2.10 Planar Couette flow

Planar Couette flow is the flow between two parallel flat plates. The shear force is constant between the plates and is described by the following expression where τ is the shear stress, μ viscosity, u plate velocity and h the gap between the plates.

$$\tau = \mu \frac{u}{h} \tag{5}$$

This can be used to calculate the torque on one of two concentric cylinders, one stationary and

one moving, assuming a small radial gap. Here u is the peripheral velocity, h the radial gap and A the mean cylinder area.

$$M = \mu A \frac{u}{h} r \tag{6}$$

2.11 Multiphase simulations

There is a lot of theory related to CFD and especially multi-phase simulations. In this section, theory relevant and specific to the simulations run, are highlighted.

2.11.1 Rotatinal motion

Two main forms of describing rotational movement are relevant for this study, MRF and RBM. In MRF the moving body and domain are stationary and the reference frame for the moving body and its close surroundings is moving instead of the body itself. The fluid that moves past it experience forces as if it were moving.

The approach of RBM is more physically correct as the geometry itself is moving in this approach compared to MRF. However, RBM is an unsteady approach and is more computationally expensive [20].

2.11.2 Overset meshing

The overset meshing method consists of two meshes, one background mesh and one refined overset mesh connected to a body [21]. It is suitable in flow with complex interactions and large displacements. Both which is expected in the flow between two gears as their interaction is both complex and displaces a large amount of fluid. The overset mesh is turned on where needed and is connected to the base mesh through an interface. In the case of RBM the overset mesh moves with the rigid body and the interface changes accordingly.

2.11.3 Time step and CFL number

The time step should be chosen as to not affect the solution. A large time step results in the fluid moving multiple cells each time step resulting in numerical errors and a poor solution. To describe what time step is suitable for a certain cell size and characteristic velocity the Courant–Friedrichs–Lewy (CFL) criteria is used. The CLF criteria is based the equation 7 where Δt is the time step, u a characteristic velocity and Δx is a characteristic length scale, often the cell width [20].

$$C = u \frac{\Delta t}{\Delta x} \tag{7}$$

For explicit solvers $C_{max} \leq 1$ prevents the escalation of numerical errors. For implicit solvers, a higher C_{max} number can be used as it is not subject to the same instability issues as an explicit solver.

In Star-CCM+ there is a adaptive time step tool that adapts the time step to fulfil a certain criteria. It ensures that the time step is small enough to resolve the flow in areas of interest.

These criteria can be based on the CFL number combined with different characteristic properties such as the convective time scale or a specific part of the flow such as the interface [22].

3 Methodology

Figure 11 is a flowchart of the methodology used in the project. In order to understand the problem, a literature study with complementary assistance from supervisors is used. Literature and assistance are the backbone for all parts in the process, as it guides every decision. Once the problem is understood it is formulated in words and a specification of requirements is constructed. Since the project is highly complex with many interacting components, it is split up into sub-problems. Multiple solutions for each sub-problem are brainstormed. The solutions are then combined, creating multiple concepts which solve the entire problem. The next step is to choose the best concept. This is done through three steps. The first is to eliminate the obviously poor/impractical solutions partially supported by tests. The second is to specify general requirements and continue with only a few concepts that meet these requirements the best. The third and final step is to choose one concept, this step can be done through a Kesselring-matrix.

Now that a concept has been decided, the design process starts. The first step is to decide what parts are to be manufactured in-house or outsourced. Components not available of the shelf will be designed in Catia V5. If components are not suitable for plastic fused deposit modelling (FDM) they will be outsourced for manufacturing. When all parts are acquired, the rig will be assembled, and stored, at Chalmers.

The rig will be validated through CFD for multiple reasons. In order to get an impression of the general flow in the test rig. To validate how well the inlet and outlet to the oil conditioning is located, both in regard to how well the temperature will be kept constant in the entire rig and to understand how the inlet and outlet affect the general flow. Finally, to get an impression of key areas where there could be oil leakage in order to prevent this.

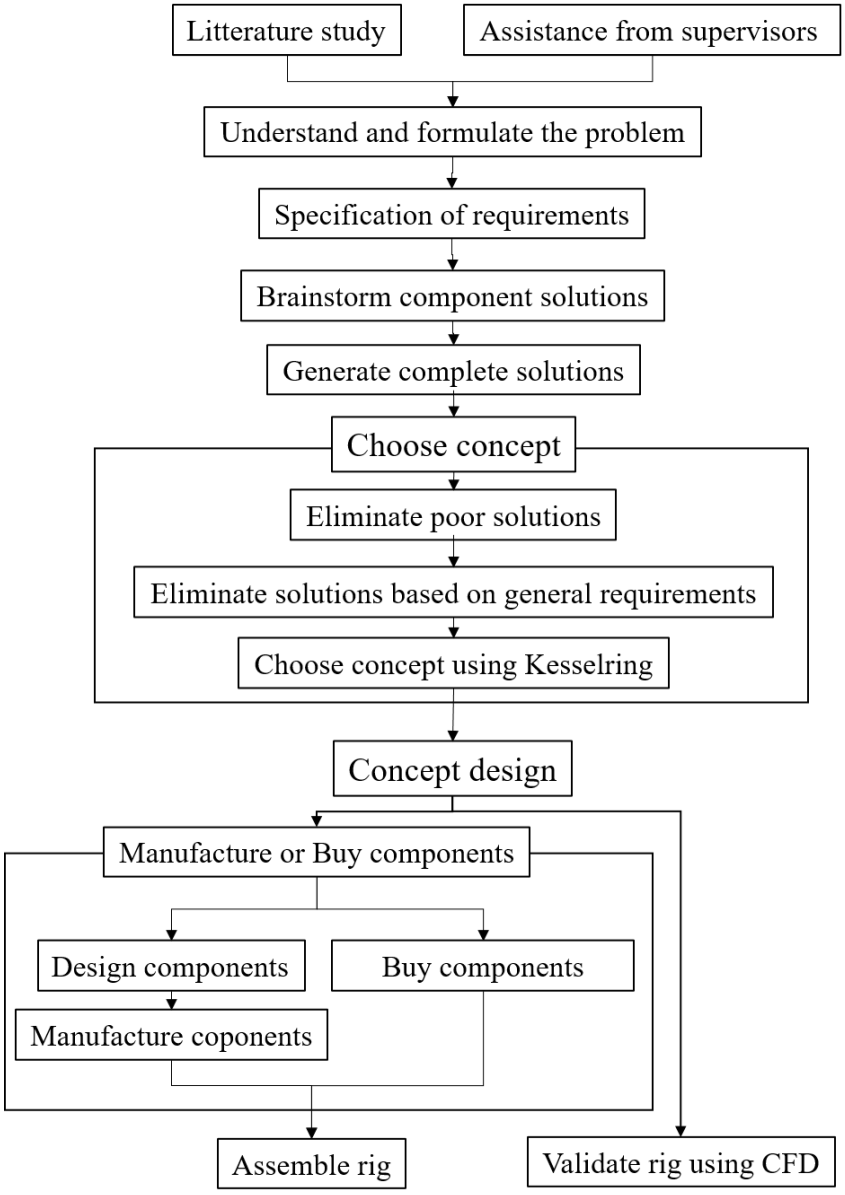

Figure 11: Project flow chart

3.1 Testing

Various simulations and experimental tests will be carried out throughout the project in order to determine what solutions and parameters should be chosen in the design process. The experimental tests will be carried out on the current test rig designed by Erwin Adi Hartono, his test rig and experiments are described in [11]. This rig will be modified so that any tests necessary can be performed. The Kistler torque sensor outputs measurements in Nm but to be able to compare the total uncertainty to Volvo's rig all measurements will be converted to watts using the relation in 8. All tests will be run at a speed of 1200 RPM as it is the speed used in most

Volvo gearbox tests.

$$\text{Power (W)} = \frac{\text{Torque (Nm) x Speed (RPM)}}{0.0095488} \tag{8}$$

Simulations regarding dynamic stability will be carried out in SolidWorks. Simulations regarding the oil flow will be carried out in Star-CCM+.

4 Pre-study test and simulation results

Component tests and simulations were done to supply information to the design process, both in terms of evaluating whole concepts and individual components. The results of these are presented below.

4.1 Test results

All tests were conducted on the existing Chalmers gear test rig with the components used in previous studies. The deep groove ball bearing test, input shaft seal test was done to assess power losses and power loss uncertainty.

4.1.1 Deep groove ball bearings total power loss and uncertainty

There are a couple of different bearing types with the most common being, deep grove ball bearings, magnetic bearings and fluid dynamic bearing. The cheapest and most readily available bearing are the deep grove ball bearings. It was chosen as the primary candidate with this in consideration. To assess the feasibility of running deep grove ball bearings tests were conducted. Three different tests were done to assess the run-in time, power consumption and the measurement uncertainty caused. All tests were done with two SKF 6004-2Z bearings connected to the existing FZG rig. The samples taken are the average measurements over 10 seconds.

For the run-in test the rig was run for one and a half hour at the speed most used in Volvo GTT gearbox tests, 1200 RPM. The run-in time was estimated to be approximately 20 minutes at 1200 RPM and a ambient temperature of 15°C.

To estimate the power consumption from the two SKF 6004-2Z bearings tests were run two times at 1200 RPM with and without the driven shaft and the bearings. The tests with the shaft only included the shaft and no gears or oil to reduce the number components with losses being measured. The data was sampled after running the rig for the previously estimated run-in time of 20 minutes. The total torque and power measurements and the corresponding addition due to bearing are presented in table 1. The power losses in the two bearings are assumed to be equal. From these tests the power consumption from one of the bearing was estimated to be around 1.86 W at an ambient temperature of 15°C.

Table 1: Bearing power losses

No Bearing		Total with Two SKF 6004-2Z bearings		Two SKF 6004-2Z bearings	
RPM	Torque [mN·m]	RPM	Torque [mN·m]	Torque [mN·m]	Power [W]
1197.6	23.7	1197.6	53.3	29.6	3.72
1200.0	23.4	1200.0	53.0	29.6	3.72

To determine the impact the ball bearings have on the repeatability the standard uncertainty was determined from 20 samples. The standard uncertainty can be extrapolated from equation 1 as the standard uncertainty for the sensor is known and the total uncertainty is gathered from the

test data. The samples were all taken after the rig had been running for the estimated run-in time of 20 minutes. The test data is presented in figure 12, where every vertical line is one test result and the test data in appendix A. The standard uncertainty from the tests were estimated to be 0.052 W which is about two magnitudes lower than the current repeatability standard uncertainty. It is however only one part of the repeatability uncertainty.

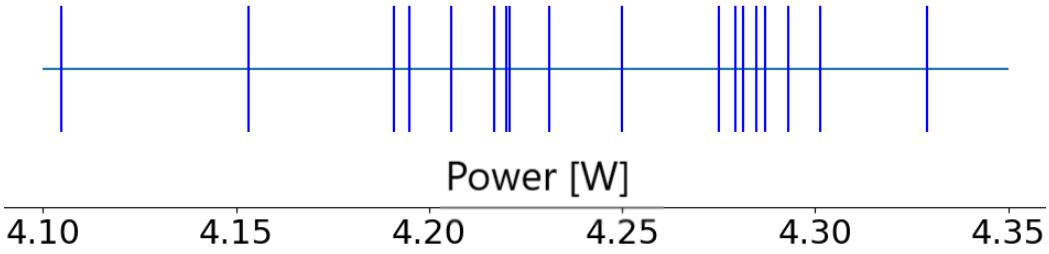

Figure 12: Measure samples of power loss in ball bearings at 1200 rpm

4.1.2 Input shaft seal power loss and uncertainty

The Chalmers gear test rig currently uses a rubber shaft seal which was measured to have a total power loss of 5 W and a standard uncertainty of 0.905 W at 1200 RPM. This test was done with oil on the seal but without any oil inside the box. This was extrapolated from equation 1 with the total uncertainty from sensor and bearing known from previous tests. A test to assess the solution with the small radial gap was conducted with results indicating sufficient sealing for RPM 100-3000 except around 600 RPM where a slow leak was observed. These leakage tests were run in the Chalmers rig with oil and where the submerged gear is also the input gear. The oil was poured in at a temperature of 18°C. The temperature was not measured under the test, but tests were run in steps ramping up to 3000 RPM and down to 0 RPM covering effects of eventual change in temperature and viscosity. This was deemed to be harsher conditions than the ones that in the new rig.

To determine the smallest radial gap without any significant effect on the results the torque difference between oil or no oil in the seal was estimated using the equations for laminar flow between two plates, equation 6. For a radial gap of 1 mm the torque delta was estimated as 0.20 mN·m (0.025 W) at 1200 RPM which is at the same magnitude as the sensor uncertainty.

4.1.3 Summary of uncertainty and power losses from components

The estimated uncertainty of all components tested are presented in table 2. These are a combination of test results, calculations and data from SKF [23]. The tests were run at 1200 RPM and the same speed was assumed in the calculations. For the uncertainty from the calculations a maximum and minimum value was possible to calculate. When transferring manufacture data to standard uncertainty numbers assumptions had to be made about the possibility that deviations could be outside this span. Hence due to possible anomalies assuming normal distribution it was assumed that the maximum and minimum values covered 95% of all measurements, i.e., equals four standard deviations.

Table 2: All component losses and uncertainties

Component	Loss		Uncertainty	
	[mN·m]	Watts	[mN·m]	Watts
Main shaft bearings (SKF 61804. SKF 61806)	7.56	0.95	0.41	0.052
Lower shaft bearings (SKF 61900. SKF 61800)	1.97	0.25	0.04	0.005
Lower shaft bearing (no oil)	1.97	0.25	0.37	0.046
Kistler torque sensor (4503A20L00B1CD1)	0	0	0.16	0.020
Radial gap seal (1 mm gap)	0.20	0.025	0.05	0.006
Radial gap seal (0.1 mm gap)	2.0	0.251	0.5	0.063
Rubber shaft seal	40.06	5.03	7.20	0.905

4.2 Simulations and analysis

Hand calculations were done to estimate a minimum permissible shaft diameter using equation 3. These results were used as an initial values for the frequency analysis. The results of these calculations and simulations are presented below.

4.2.1 Shaft bending

A finite element analysis (FEA) were done before and after the frequency analysis presented in section 4.2.2 to ensure that the shaft bending and stresses did not exceed the design values. The results from the first FEA with a ∅20 mm resulted in a maximum deflection of 0.18 mm and less than 0.1 mm at the back wall. The requirement at the back wall was the main limiting factor as too much deflection there would result in no gap in the radial gap seal. This suggested that a diameter of ∅20 mm would be sufficient to not get any interference with the sealing solution. The maximum Von Mises stress was 24.3 MPa located close to the first bearing, similar to what is indicated by the leftmost green arrows in figure 13. This is less than one fifth of the yield stress for all shaft steel and was deemed sufficient.

An additional simulation to evaluate the new deflection and maximum stresses were done with the new minimum shaft diameter of ∅32 mm from the frequency analysis. The new results showed a maximum deflection and Von Mises stress of 0.027 mm and 15.8 MPa respectively, see figure 13.

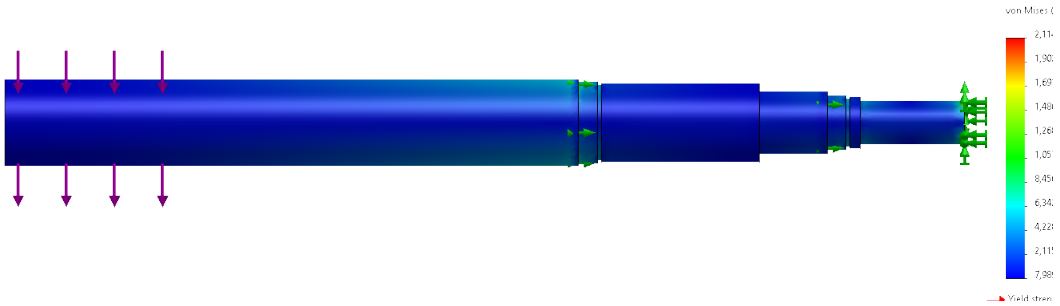

Figure 13: First bending mode with ∅32 mm

4.2.2 Frequency analysis

The components most susceptible and probable to experience large forces due to oscillations at the resonance frequency are the upper and lower shaft assemblies. They are also both connected to the torque sensor and oscillations could affect the results as described in section 2. To prevent any incorrect torque readings or rig damaging oscillations both shafts were designed to have a resonance frequency 5% higher than the maximum rotational frequency for the corresponding shaft. One difference between the shafts is that the lower shaft is dampened by the oil as it is always in contact with the oil in the sump. However, to ensure reliable operation with low oil levels both shafts were designed with the fore mentioned design criteria in mind.

For the main shaft, the maximum frequency is 50 Hz (3000 RPM) and for the lower shaft it is 121 Hz (7263 RPM) due to gear ratios. To estimate this frequency a frequency analysis tool available in Solidworks 2020 was used. The first bending mode for the main shaft is presented in figure 14. The bearings were modelled as elastic supports with a stiffness of 400e6 N/m. The analysis resulted in new minimum shaft diameters of ∅32 mm and ∅20 mm for the main shaft and the lower shaft, respectively.

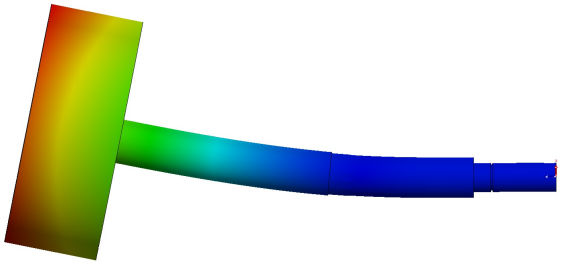

Figure 14: First bending mode with ∅32 mm

5 Concept design and selection

Many different solutions for each rig function were created. These were compared in regard to how well they fulfilled the design requirements using a Kesselring matrix. The design requirements have weighs corresponding to their importance. The Design requirements are based on a combination of requirements from Volvo and Chalmers and are described in detail in section 1.3. In this section the concepts and the differentiation's identified when comparing the concepts are presented.

5.1 Components contributing to uncertainty in power loss measurements

In this subsection the selection of components and concepts directly effecting the power loss uncertainty is discussed.

5.1.1 Shaft configuration and design

Due to the test object requirement being a gear paring and not multiple gears per shaft a solution with the shafts only supported on one side was chosen, see figure 15a. The shaft supported on a single side have an inherent moment acting on the shaft increasing the stress in the shaft and the force on the bearings. But as the gears are not subject to any other force than the torque from the oil and bearings the single sided shaft approach was possible without an inhibiting increase in shaft diameter and bearing size. A shaft only supported at one side have the benefit that the rig operator does not have to remove one shaft support in order to access and change the test object reducing the downtime between tests.

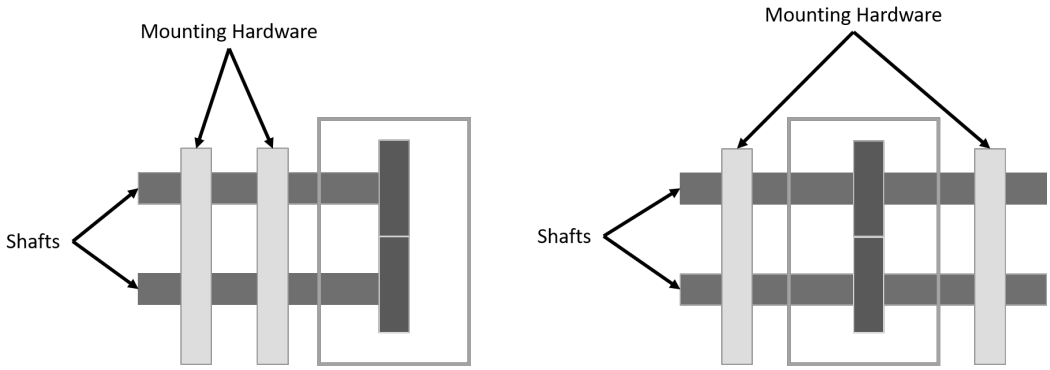

(a) One sided shaft support (b) Two sided shaft support

Figure 15: Shaft support configuration options

The driven shaft can be either the upper or lower one, as there is no desire to do tests with a moment applied on the counter rotating shaft in this rig. Driving the lower shaft has the benefit that a single gear can be tested in the rig and isolate the churning losses from counter shaft gears, see figure 16a. However, in a real I-shift gearbox the gears are always connected in pairs and rotating together. The benefit with a driven upper shaft is that the lower shaft can be mounted inside the box. In some hilly conditions the lower shaft can be partially submerged and driving the upper shaft eliminates one contact seal if the lower shaft is mounted inside the

box, see figure 16b. A contact shaft seal has a friction loss proportional to the peripheral speed [24]. Every loss can be compensated for afterwards but it also has associated measurement uncertainty and a decision was made in agreement with the supervisors at Volvo to not test a single gear and increase the measurement accuracy of a pair instead.

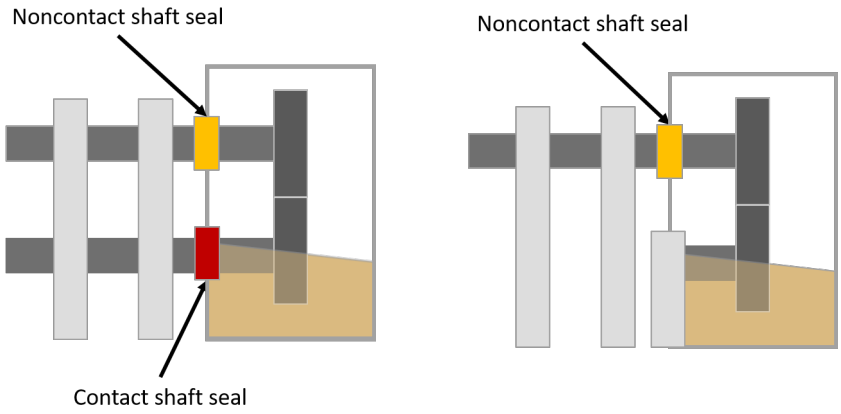

(a) Lower shaft driven (b) Upper shaft driven

Figure 16: Input shaft configurations

The required shaft diameter was determined by first analysing the deflection in the shaft as described in section 4.2. Those two shafts was then run through a frequency analysis which resulted in a new larger smallest permissible diameters, the analysis is described in section 4.2.2. These smallest allowed diameters were chosen as the shaft diameters for each respective shaft as this allows for the most space for mounting options.

5.1.2 Seals

Sealing the box with the fewest contact seals possible is important as they are a big source of losses and power loss uncertainty which is described in section 4.1.3. Labyrinth seals and small radial gaps are better when trying to minimize losses and is suitable for the upper shaft which will only experience oil splashes. A small radial gap combined with oil splash protection was chosen as the sealing solution as it is the cheaper solution and tests described in section 4.1.2 indicate that it is sufficient as a solution. To prevent oil collecting in the splash protection a drainage slot was added with its own splash protection. A small rubber ring was also added to prevent oil to run along the shaft, as illustrated in figure 17. This splash protection not only helps to seal the box, but it also reduces the effects of oil interacting with the upper shaft.

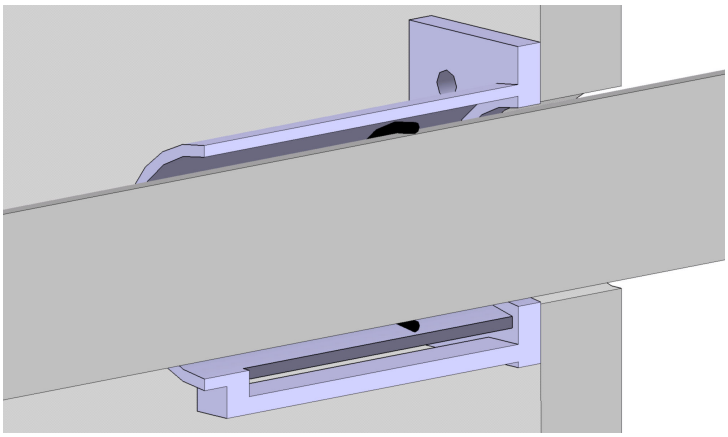

Figure 17: Section view of the shaft seal mounted on the inside of the box

For the lower shaft the choices in bearing type and bearing configuration described in section 5.1.3 enables the lower shaft seal to be removed completely where else a contact seal would have been necessary.

5.1.3 Bearing types and configuration

As the gears are rotating there is a need for bearings, three main solutions were investigated, traditional ball bearings, magnetic bearings and hydrodynamic bearings.

Hydrodynamic bearings offer a compact low friction solution with little variation between rotational speeds. This is due to the fact that there are no contact between the shaft the bearing. A complete air bearing solution supplied by IBS Precision Engineering Ltd using New Way Air Bearings bearings was considered which included four bearings, housings and a air filtration system. The air filtration is needed because their bearings deliver the air through a porous media and industrial compressed air can contain particles and oil that can get stuck in the porous media and reduce the performance of the bushing over time.

Magnetic bearings offer the same benefits as the hydrodynamic bearing as there is no contact between the rotating and stationary parts. Similarly, they both have negligible change due to wear and as previously mentioned very small differences related to different speeds. Most commercial solutions for magnetic bearings are for much larger applications than the rig currently being designed. They are also not readily available as of the shelf components which is prohibitively in a project with this time span.

The traditional deep grove ball bearing has higher losses than the previous two option but has many benefits. Deep grove ball bearing requires no additional supply of air or power and is readily available in many configurations and sizes. Due to this it is also the cheapest option at less than a one-hundredth of the price for an air bearing solution. It is also the most compact and is the only solution that enables the lower shaft support to be moved into the box removing one contact seal. From the test results presented in table 2 it is clear that not having to use a contact seal significantly outweighs the power loss and uncertainty introduced by the deep grove ball bearings and it was therefore chosen option.

The compactness of the deep grove ball bearings also enables the bearings to be moved inside the lower gear and eliminate all effects of the lower shaft interacting with the oil and air, see figure 18.

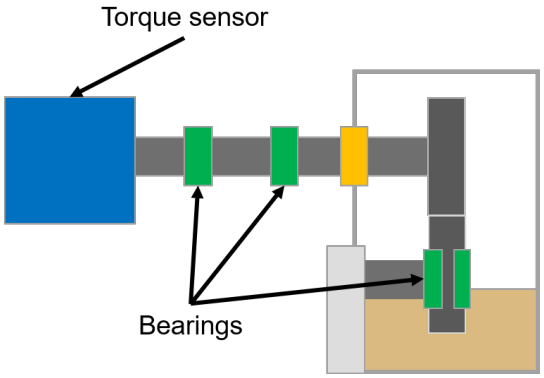

Figure 18: Concept including deep grove ball bearing and the Kistler torque sensor

5.1.4 Torque sensor

To reduce the error in the torque measurements the error sources can be reduced in size or removed. For the torque sensor two concept were considered, using the original Kistler torque sensor and trying to reduce the error sources or integrate the torque sensor into the upper shaft and eliminate the error from the bearings which are discussed in section 5.1.3.

Integrating the torque sensor in the shaft would require a custom-built solution to be designed and manufactured. The cost for this was estimated to be between 50 000-100 000 SEK per sensor. Using this approach would eliminate the upper shaft bearing errors. This solution combined with a non-rotating lower shaft is presented in figure 19a. To completely eliminate bearing losses and uncertainties an additional sensor on the lower gear is needed. In this case both sensors includes the torque from the lower bearings the difference is the torque from the oil, see figure 19b.

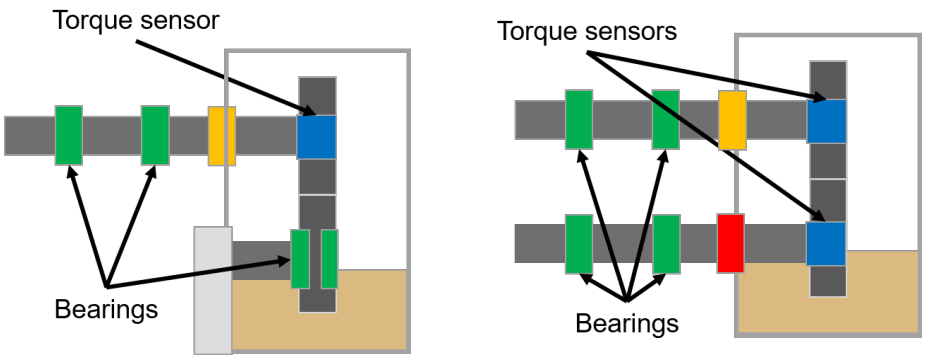

(a) One integrated torque sensor

(b) Two integrated torque sensors

Figure 19: Options including custom built torque sensors

The other approach is to use reliable and predictable bearings with low power loss uncertainty in combination with the original Kistler torque sensor. After the bearing run in and uncertainty tests presented in section 4.1.1 it was deemed that the deep grove ball bearings were predictable enough to not significantly affect the power loss uncertainty goal of less than 55 W negatively. This solution is presented in figure 18,

5.1.5 Mounting system for gear wheels

The gear retention and mounting system effects the readings, safety and usability of the test rig. The gearbox consists of two types of gears, those that is mounted on a shaft and those that are machined straight onto a shaft. Mounting the gears in the rig presents two main problems, adjusting the gears to fit on the shaft and how to fix the gears on the constant shafts.

Concepts for fitting test objects included conical shafts, interchangeable shafts or modifying existing gears or manufacturing new gears. These four concepts can be seen in figure 20. The conical shaft was excluded because the axial centre of different gears are different which makes oil level readings more complex and prone to errors. It also is the bulkiest of the four solutions as all other solutions can be contained within the gear. As the gear would be clamped against the cone the axial positing is also prone to change with wear.

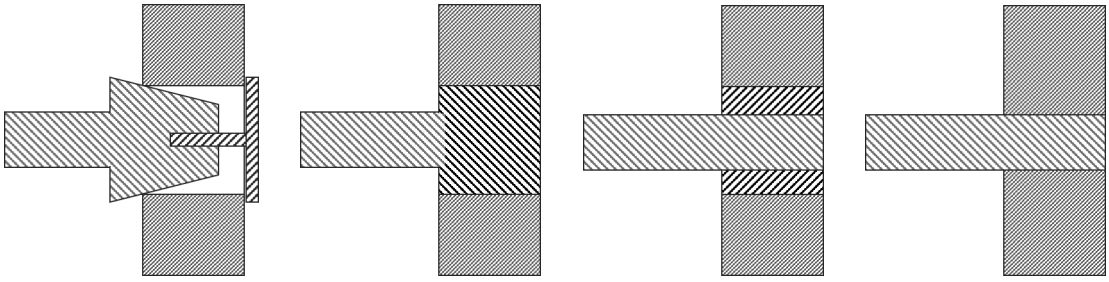

(a) Conical Shaft (b) Different Shafts (c) Modular system with constant shaft (d) Constant shaft New Gears

Figure 20: Concepts for gear-shaft interface

As there are integrated gears there is a need to manufacture completely new test objects. Interchangeable shafts are not needed with the custom test objects as they can be designed to fit on any shaft diameter small enough to not affect the gear teeth. Similarly, if the original gears are modified to fit on another shaft diameter it can be any diameter smaller than the inner diameter of the gear wheel. Modified gears and custom gears were selected as the solution for its minimum effects on the results and its flexibility.

Fastening mechanisms consisting of clamps and screws in different configurations were considered. Screws introduces more lose components while the clamps can be mounted on the shaft. The clamps are also more user friendly as is much easier to see if they are fastened correctly but this comes at a cost. The clamps are a bulkier solution with a more complex geometry having a larger and more unpredictable effect on the oil flow compared to the screws. There also are safety concerns with the clamps as they fail much faster and less gradual than screws

unscrewing. The main goal of the study is to reduce the power loss uncertainty and the solution including the screws were the best in that regarded and chosen on those grounds.

5.2 Components affecting functionality, usability and repeatability.

In this the design choices of components linked to usability, repeatability and other design requirements is discussed.

5.2.1 Box design

The design of the box affects the usability and capability of the rig. All boxes should be able to include the real gearbox housing inner wall profile and different options such as a oil gutters. A correct inner wall profile is needed as it effects the radial flow. The inner wall profile is not constant through the length of the gearbox and modifications might be tested and thus different inner profiles inserts must be mountable inside the box, see figure 21 for a example. The design concepts focus on different methods for accessing the gears. The length of the box in the axial direction was based on results from previous Volvo CFD simulations that indicated that 80 mm was enough to make the effects of the axially located walls negligible. The concepts were a top access hatch, a front access hatch and removing the whole box, these are presented in figure 22. Variants of these concepts where also considered with partial access hatches and different ways to remove the box.

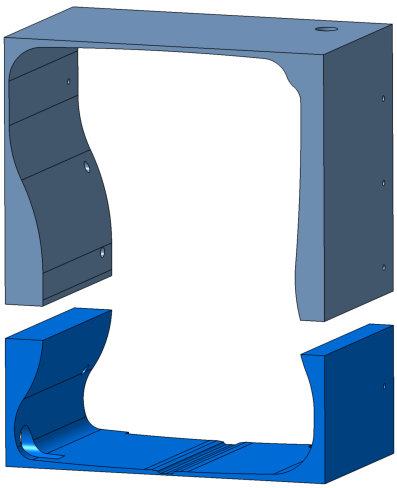

Figure 21: Example of gearbox profile box inserts

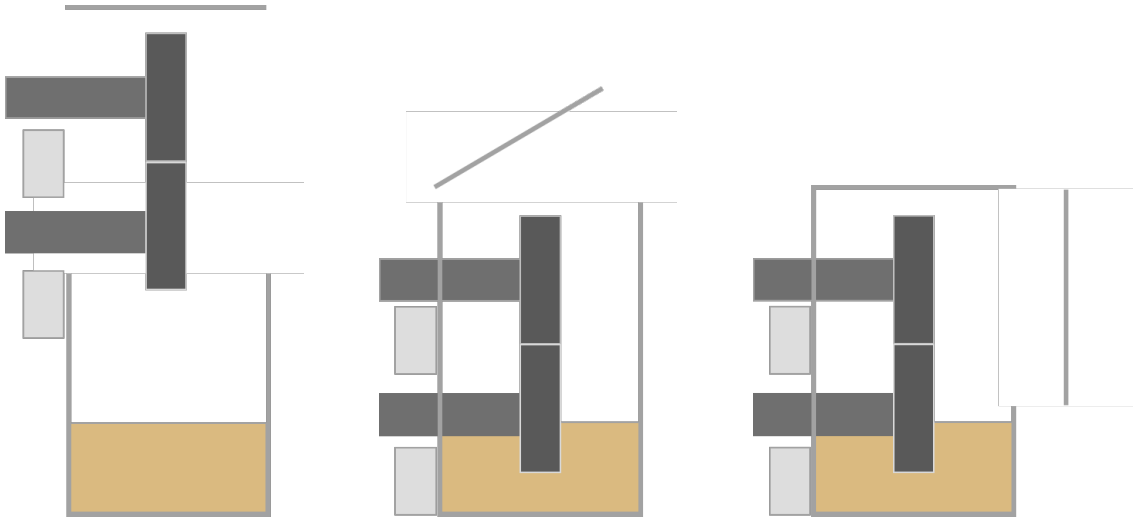

(a) Removable box (b) Top access hatch (c) Partial front access hatch

Figure 22: Box concepts

Removing the whole box from underneath has the benefit that only the gears have to be cleaned between tests assuming there are multiple boxes with different types of oil in standby. In the case of multiple it also makes it possible to switch inner wall profiles and other options while the rig is running reducing downtime. This however adds a lot of complexity and potential points of oil leakage. As oil leakage has been a big problem with some previous rigs this solution was not investigated further.

The box with a access hatch on the top has the benefit that the oil leakage from opening the box and changing gears is kept at a minimum as there is no risk of dropping the box and spill oil. The drawback with this is the ergonomics. The box will be more than 40 cm deep and the heaviest gear on that shaft is around 10 kg. This makes it difficult to access and lift the gears up from the box and keep good lifting ergonomics [25]. There also is a problem with inserting different inner wall profiles other optional modification at the bottom of the box as there are two shafts in the way.

A box with an access hatch on the front starting above the expected oil level was the chosen option. The maximum oil level here being at the distance from the wall which is 80 mm from the widest gears side. It applies for the normal oil fill levels, 16l in a real gearbox for any hill condition up to $\pm 11.3°$. This keeps the benefits of the top access hatch regarding oil spill and greatly improves the ergonomics as this box makes a better lifting posture possible [25]. However, it introduces a thin line of obstructed view through the front access hatch. The mean shaft height above the floor was chosen to be 105cm which is in the middle of the optimum lifting height span for heavy objects for the majority of Swedish people [25]. Is also makes it easier to insert inner wall profiles and other options compared to the box with the top access hatch.

5.2.2 Oil level and conditioning

The oil level is affected by its thermal expansion and aeration level which makes consistent readings of the oil level hard to achieve. Three different oil level measuring systems were considered, visual readings of the oil level, capacitive fluid level sensor and using a pressure sensor to measure the oil level.

Visually assessing the oil level can be done in two ways, on the side of the box, internally or outside the box, externally. Taking readings of the oil level outside the box has the downside of adding more oil to the system making emptying the box more difficult. It does have one advantage which is removing aeration from the error sources as the external oil can be sealed of during tests and opened for measurements. However it is still subject to errors from thermal expansion. Being able to visually read the oil level is also needed to get an initial reference for the two later options and external visual readings were the concept chosen.

The capacitive oil sensor has the benefit of being integrateable into a computer system and suitable for remote monitoring. However, questions about the effects of temperature and thermal expansion on the dielectric constant and capacitance are introduced. Furthermore the dielectric constant changes between oils which makes recalibration necessary when changing oil type[26]. Assessing these effects was deemed outside of the scope of the project and was not further investigated.

The pressure sensor has the benefit of adding remote monitoring capability. It also has the benefit of not being sensitive to thermal expansion and aeration as the weight of the oil is the same and the pressure at the bottom will be the same regardless. Densities of oils are also more readily available reducing the amount of recalibration work. However, a sensor with a accuracy of ± 0.09 mBar is required to achieve a level measurement accuracy of ± 1 mm. These exists, for example a Paroscientific 202BG is able to fulfil the aforementioned requirements with a precision of ± 0.015 mBar (± 0.17 mm) and is available from Ole A. Nordby AS at a cost of 75 000 NOK.

To get to and keep the oil at the desired viscosity good control of the oil temperature is needed. Instead of designing a new oil conditioning system the rig was designed to be able to accommodate the Volvo GTT oil reconditioning system presented in section 1.2.1. Volvo GTT have already developed a oil conditioning system with the performance required and offered to lend a unit when the rig is running tests for Volvo GTT.

5.2.3 Tilting mechanism

It is essential to test the gearbox at different inclination angles as it has a large effect on the oil flow inside it. Three different concepts adding tilting functionality were considered. These where height adjustment boxes, a hydraulic tilting system and an actuator tilting system, all of these are shown in figure 23.

Putting height adjustment boxes under the front or back to pitch the rig is the simplest conceptually solution and gives excellent repeatability. It does however require an overhead crane or similar to safely lift the rig when positioning the boxes adding complexity and building requirements, see figure 23a.

A hydraulic system has the benefit of being completely integrateable into the rig compared to the height adjustment boxes. This solution is however much more complex and expensive as both a cylinder and a hydraulic pump is required. There also is the potential safety risk of the rig pitching if a sudden loss of oil pressure occurs.

An actuator, manual or electrical is simpler, safer and cheaper compared to the hydraulic system and safer than height adjustment boxes. The height adjustment boxes require lifting on side of the rig which is a safety risk every time it is performed. There also is the possibility of faulty box placement and the rig falling over as a result of that. No similar operator error is possible with the actuator. Compared to the hydraulic system much fewer components are required and for this low load case especially in the case of a manually operated actuator.

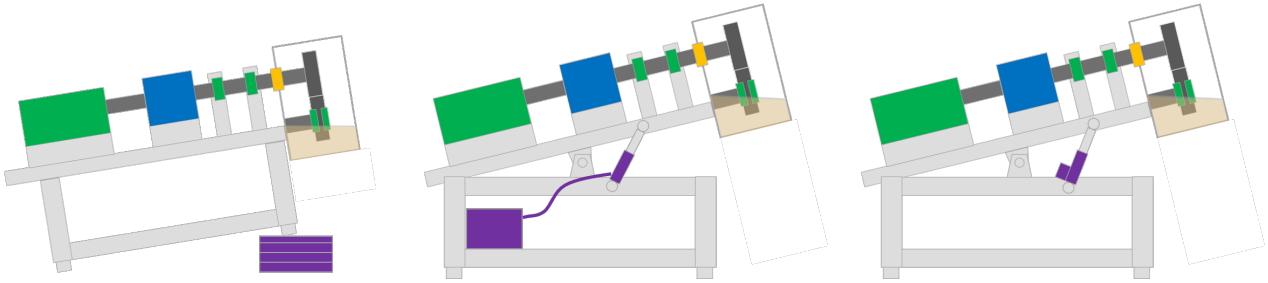

(a) Height adjustment boxes (b) Hydraulic tilt system (c) Actuator tilt system

Figure 23: Tilting concepts, purple indicates components related to the tilting concept

5.2.4 Electrical system and monitoring

Redesigning the electrical system was deemed outside of the scope of this study. The choice was made to carry over all the electrical components and the Labview software to the new rig. The oil conditioning system is supplied by Volvo GTT as a turnkey solution.

6 Selected Concept

The concept selected share many parts with the Chalmers rig used for earlier studies at Chalmers University of Technology but is modified to accommodate the testing requirements specified by Volvo, see figure 24. For example, the motor, base plate and torque sensor from the Chalmers gear test rig is reused in the new rig. The Kistler torque sensor in the test rig is calibrated and has a claimed standard uncertainty better than 0.02 W (0.00016 Nm) at 1200 RPM which is a significant improvement compared to the 5 W standard uncertainty of the HBM T12 used in the Volvo gearbox test rig.

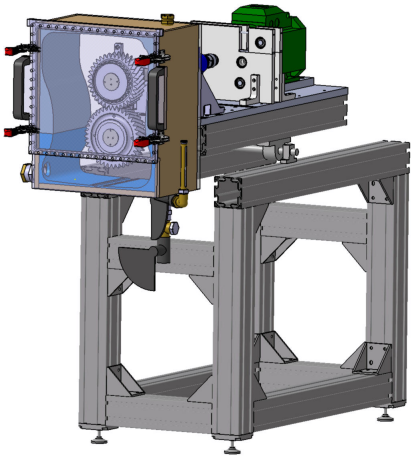

Figure 24: CAD model of new rig

6.1 Electrical System

The electrical system is the one from Chalmers gear test rig with the addition of the oil conditioning rig and included software. The Chalmers electrical system consists of a computer running software based on LABVIEW connected to a multifunctional DAQ device from National Instruments (product number: USB-6221). The multifunctional DAQ device is connected to an ABB motor (variant number: 3GAA091313) through a Mitsubishi inverter (variant number: FR-D740-11K). The multifunctional DAQ device is also connected to a Kistler torque sensor (Variant number: 4503A20LOOB1CD1). The Oil conditioning system is controlled directly by the computer which is running software provided by Volvo. A block diagram of the system is shown in figure 25.

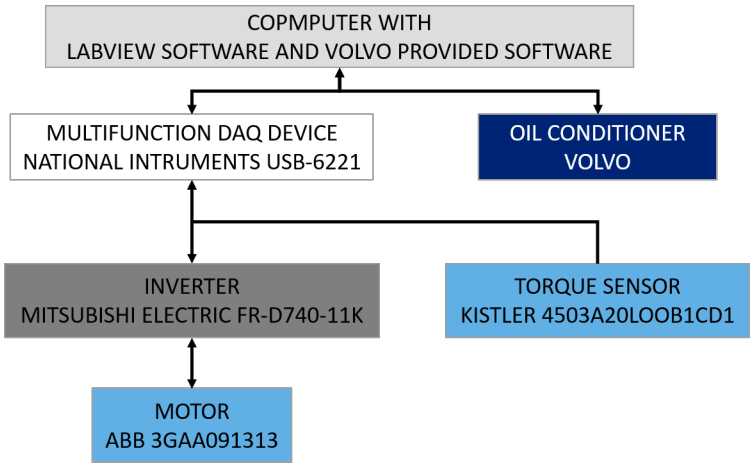

Figure 25: System Block Diagram

6.2 Shaft configuration and box design

Compared to the Chalmers rig the new design has been modified to accommodate the larger intershaft distance of 160 mm currently in use in the AMT gearbox. The shafts are not the same as in either previous rigs but has been designed to accommodate the gears from a Volvo trucks AMT gearbox. They are also configured to minimize the leakage risk and associated uncertainties. The lower shaft is fixed to the box, eliminating one possible leakage point and uncertainties from one shaft seal, see figure 26. However, the lower gear still needs to rotate, thus two bearings have been placed on the lower shaft inside the gear.

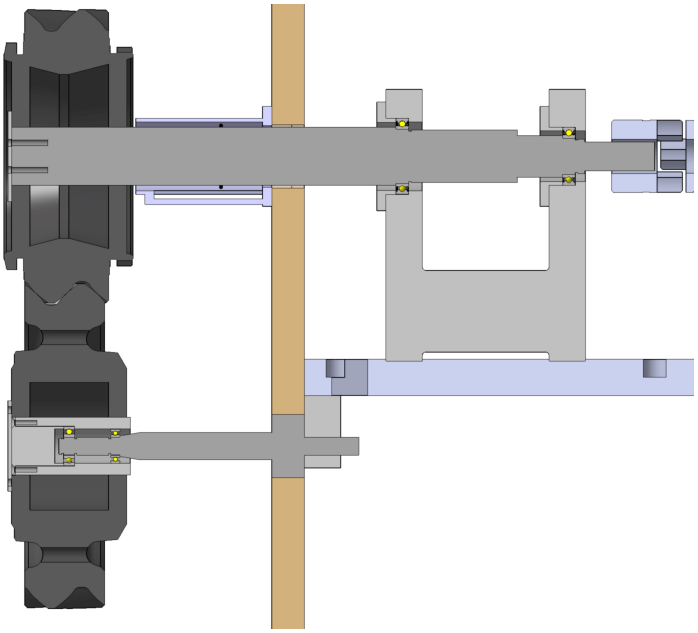

Figure 26: Shaft configuration with arrows indicating direction of communication

For faster access to the gears the screw on front plate on the Chalmers rig have been replaced by

a magnetic hatch. The box also includes clamps for further securing of the hatch. As can be seen in figure 27 not the whole front is removable resulting in that the box doesn't have to be emptied when opening the box to change the test setup, a feature which the current configuration of the Chalmers rig did not include. It also has a hole on the top and a ball valve on the bottom which enables filling or emptying of oil when the hatch is closed and when the rig is running, again an improvement compared to the Chalmers gear test rig. All sides of the box including the hatch are transparent PMMA to make high speed photography and manual visual observations possible. The four sides indicated by brown in figure 27 are visually obstructed by the wall profile inserts if present, however, these can be removed if radial observations are desired. Example of insert design can be seen in figure 21.

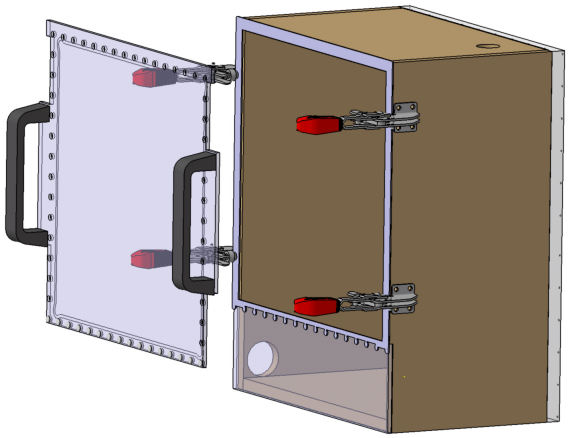

Figure 27: Hatch

To be able to simulate hilly running conditions the rig will be tiltable to $\pm 11.3°$ from the installation angle using a motorized linear actuator system. This is a feature that the existing Volvo test rig has but not the Chalmers rig where the test chamber was fixed to the base structure.

6.3 Oil conditioning system and level indicator

The oil conditioning is done using an external unit supplied by Volvo similar to their existing system, see figure 5. The oil conditioning rig is controlled using the Controller Area Network standard (CAN) and must be supplied with 24V DC, hot and cold water. The output is conditioned oil which is then feed into the box through 1 1/2" hole. The hole size is this large to minimize the inlet velocity. The oil returns to the oil conditioner through a hose connected a hole in the opposite corner of the box. This is to force the oil to mix as much as possible inside the box so that the oil is the correct temperature and viscosity everywhere, see figure 28 for a section view with the inlet and outlet highlighted. To measure the extent of oil mixing and spreading between inlet and outlet a CFD simulation was run.

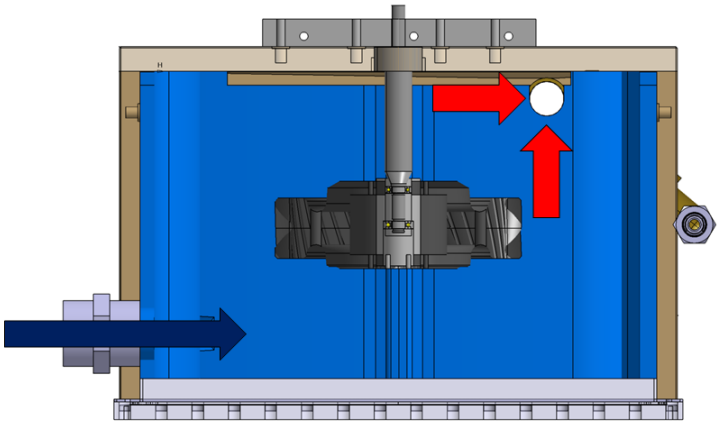

Figure 28: Section view of the box with the conditioned oil inlet and outlet highlighted with blue and red arrows respectively

To ensure that the oil level stays consistent between tests, an external sight glass level gauge replaces the current plastic hose in use today at Volvo. The straight transparent sight glass enables measurements at the gear center line and the rigidity of the component enables more consistent readings compared to the flexible plastic hose. Similar to today the sight glass can be isolated with a valve so that it is not affected or affecting the oil being moved and aerated by the gears. A figure of the system is presented in figure 29.

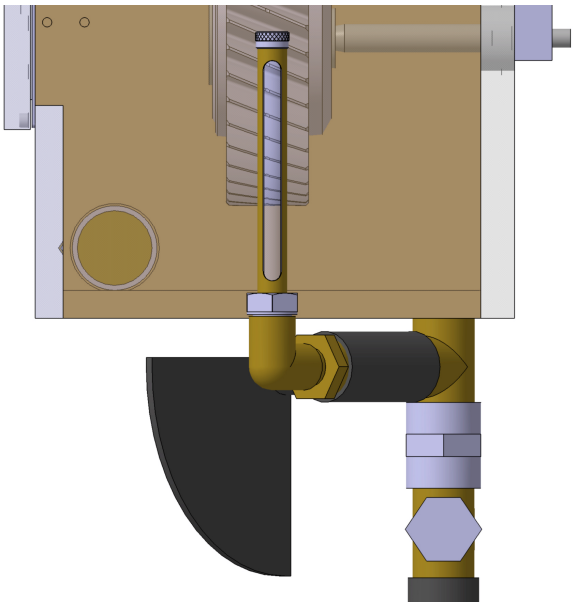

Figure 29: Oil level measuring system with sight glass level gauge

6.4 Safety

A risk assessment for the concept was conducted to ensure safe operation of the rig. The identified risks were obtained using the Swedish Process Safety Association (IPS) guidelines for assessing tolerable risks in chemical handling industry [27]. Using the guidelines all risks, except the ones concerning the oil, were deemed tolerable.

In a real gearbox the can oil reach temperatures of 80°C or higher, a temperature at which water cause 3rd degree burns in less than one second of exposure [28]. Oil, however, has a lower specific heat capacity of around 2 KJ/kg compared to water which has a specific heat capacity 4.18 KJ/kg. Still, the decision was to remove the risk completely and limit the oil temperature to 44°C or less at which multiple hour exposure is required to get any sustained skin damage [28]. Due to environment and health concerns, cooking oil or food grade oil will be used when possible.

6.5 Drawings of designed test rig

For technical drawings of components designed in the study see appendix B.

7 Validation through CFD

Now that the concept is selected, parts of it can be validated through CFD. To do this a watertight surface model is required. Such a surface model is then used as a domain on which boundary conditions are set and meshing is done. Thereafter the physics model is set up, as well as reports and monitors. The simulation is then run. Once it is processed, it is first checked for convergence. Assuming a good convergence the simulation is post processed to acquire all relevant information about the flow. These steps and the exact selections are discussed in the chapters below.

7.1 Surface model

A surface model is established based on the inside of the 3D Catia V5 Assembly seen in figure 30a. The surface model is simplified in order to be more fit for a simulation, see figure 30b. First, only the internal surfaces are of interest, therefore any geometry on the outside are erased as they have no effect on the flow. The simplifications present on the inside are on the front wall as well as on the two gears. The front wall is flattened as compared to the real design where there is a gap around the hatch. Oil at the hatch edge is already expected and leakage here is prevented by a contact seal. This is contrary to the radial gap seal where the flow is unknown. If the gap was included there would be a need to solve the flow in there which is comparatively small at 1 mm. Having enough cells to accurately capture the flow would require a concentration of cells. The combination of relatively high computational cost and knowing the flow not being a necessity resulted in it being excluded from the simulation domain.

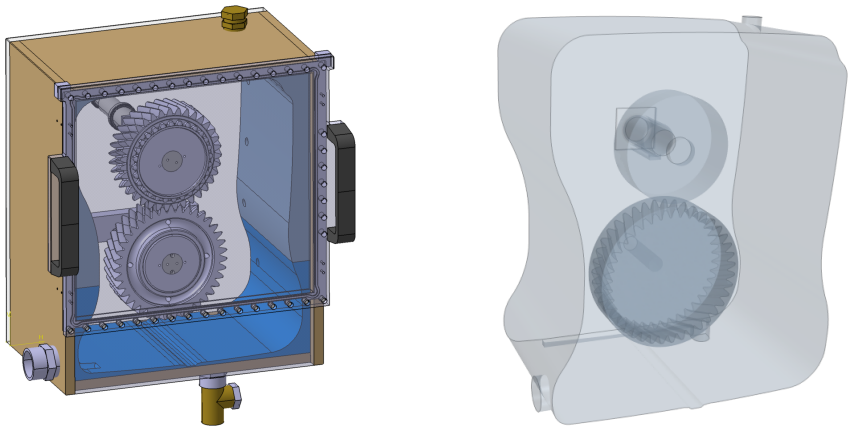

(a) Before modifications (b) After modifications

Figure 30: Simplifications made on the box assembly

The lower gear was simplified such that the sides are cut off by straight walls instead of the complex geometry in the assembly, for a comparison before and after the simplification, see figure 31. This simplification is justified by the fact that the original geometry would need a very large amount of computational mesh cells to get a good representation of the area. The change was expected to only affect the flow in a minor way from observations done when

performing the tests described in section 4.1. The cell requirement weighs heavily as there is a strict limit in RAM memory of 16 GB on the computers running Star CCM+. The upper gear was simplified to a cylinder without teeth, justified by the fact that the flow between the gear teeth is of little interest. This allows the domain to be meshed without an overset mesh or prism layer shrinkage. Such methods would otherwise be necessary since the space between two rotating gears becomes very small when the teeth interact.

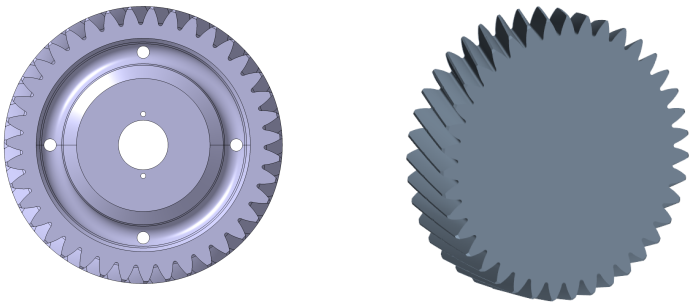

(a) Before modifications (b) After modifications

Figure 31: Simplifications made on the lower gear

The surface model needs to be impermeable which, when simplifying a model in Catia V5, cannot be guaranteed. To solve this, a surface wrap is performed on the imported surface in Star CCM+.

7.2 Interface and boundary conditions

Now that the surface model is complete, there needs to be an interface between the rotating gear and the bulk volume. This interface defines what part of the mesh will rotate, simulating the rotation of the gear. The rotating mesh uses a Rigid Body Motion (RBM) model as it is proven to generate significantly better results compared to the alternative Moving Reference Frame (MRF) in this type of simulations [29]. The rotation speed of the lower gear is set to 600 RPM. This speed is about the lowest a gear on the lower shaft would experience under a prolonged time. The lowest speed would hypothetically transfer the least kinetic energy to the oil and hence result in the least mixing i.e. the configuration most sensitive to the inlet and outlet flow. It is also the speed at which the most oil leakage occurred at during small radial gap seal test.

Three different simulations where set up. The boundary conditions of the upper gear and upper axle was set to rotating wall with no slip in all simulations. The rotational speed is based on the true gear ratio of 39 teeth over 35 teeth resulting in -668.57 RPM, negative as it rotates in the opposite direction of the lower gear. The Interface around the lower gear was set to wall with a slip condition in all simulations, this effect is only important for cells which fail to connect between the two regions. The difference between the simulations is the boundary conditions on the bottom and side holes, seen in figure 32. The different combinations are found in table 3.

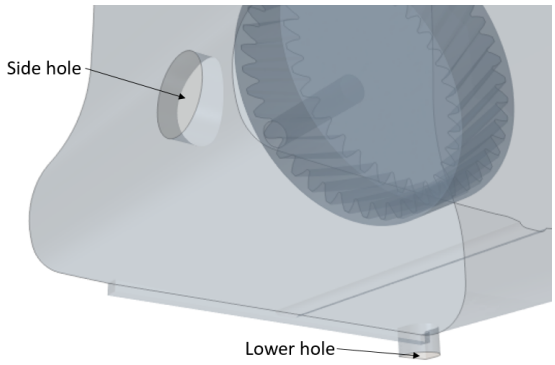

Figure 32: Inlet and outlet hole boundaries

Table 3: Boundary conditions for the inlet and outlet holes

Simulation number	Lower hole	Side hole
1	*Wall, no slip*	*Wall, no slip*
2	*Mass Flow Inlet, -0.0537 kg/s*	*Mass Flow Inlet, 0.0537 kg/s*
3	*Mass Flow Inlet, 0.0537 kg/s*	*Mass Flow Inlet, -0.0537 kg/s*

All remaining, unmentioned, boundaries are wall boundaries with a no-slip condition in every simulation.

7.3 Mesh

The domain is meshed with the validation targets and limited resources of RAM in mind. The RAM restricts the mesh to an upper limit of around 7 million cells. The entire domain consists of 6.88 million cells, an overview can be seen in figure 33.

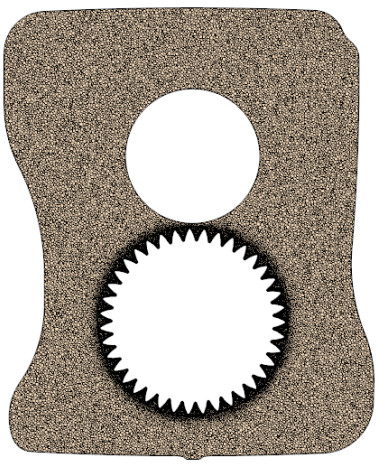

Figure 33: Overview of the mesh

The selected meshers and edited default controls are found in table 4 and table 5 respectively.

Table 4: Selected meshers

Surface Remesher
Automatic Surface Repair
Polyhedral Mesher
Prism Layer Mesher

Table 5: Default controls that have been edited

Setting	**Value**
Base Size	2.4 mm
Target Surface Size	100%
Minimum Surface Size	80%
Surface Growth Rate	1.25
Number of Prism Layers	3
Prism Layer Stretching	1.25
Prism Layer Total Thickness	1.9 mm
Volume Growth Rate	1.25
Maximum Tet Size	85%

Besides these options there is a surface control disabling prism layers on all surfaces except the lower gear, as well as two volume controls used for refinement. The first volume control refines inside the interface of the lower gear as this is where the largest gradients can be expected in the flow. The gradients appear because of the large relative velocity between the rather still bulk fluid and the rotating gear. The mesh inside the interface is refined with 0.8 mm polyhedral cells, see figure 34a. Inside the interface there are 3.43 million cells. The second volume control is around the upper shaft and shaft shield, see figure 34b. The cells there are 1.2 mm, to get a better understanding of how much oil will be collecting in the area. When the amount of oil is known, the risk of oil leakage out of the rig can be determined.

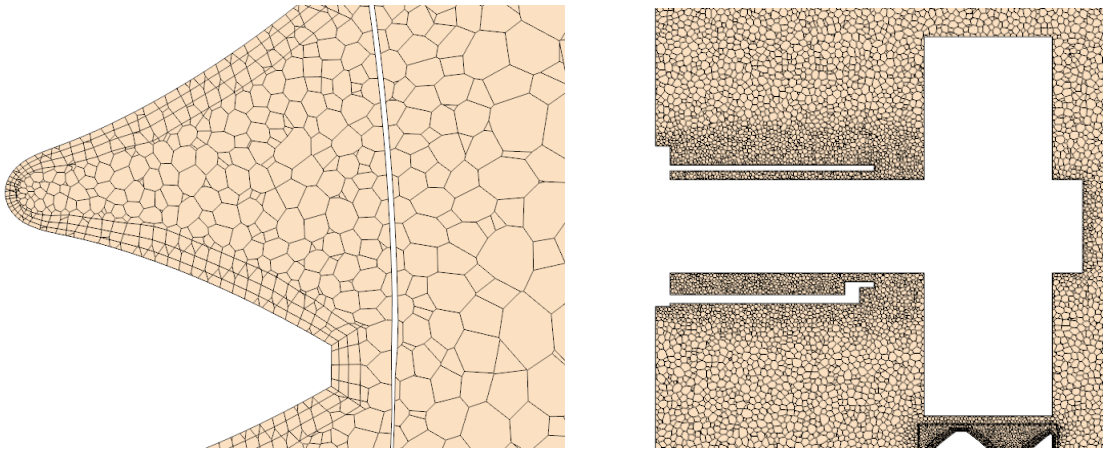

(a) Zoom in on mesh near the lower gear and interface

(b) Side view of the upper gear, axle and axle shield

Figure 34: Refinement zones of the mesh

7.4 Physics

The maximum time step was calculated so that any fluid in the domain will travel at maximum one cell per time step. The maximum velocity in the domain is the radius of the gear times the rotational speed. The overall cell base size was used as the maximum distance to travel for one time step. The time step was chosen with this and a safety factor of 1.3, resulting in a time step of 2.5e-4 s. Even though the maximum time step alone does not ensure that the CFL number criteria is fulfilled, the time step is also adaptive with a free Surface CFL condition ensuring a CFL number ≤ 0.4 at the interface if it can be achieved with a time step larger than $5.0\text{E}-6$ s. Thus, the CFL number requirement discussed in section 2.11.3, should be fulfilled. However, the exact solution near the lower gear is of marginal interest. More interesting is the general flow field in the bulk flow. This justifies the larger maximum time step.

A complete list of the selected models for both phases, oil phase and air phase are presented in, table 6. Gravity is directed straight down meaning no tilt is simulated.

Table 6: Physics Models

(a) Common

Physics Model
Three Dimensional
Gravity
Implicit Unsteady
Multiphase
Multiphase Interaction
Volume of Fluid (VOF)
Multiphase Equations of State
Segregated flow
Gradients
Turbulent
Reynolds-Averaged Navier Stokes
Wall Distance
Segregated Fluid Isothermal
Adaptive Time-Step
Solution Interpolation
K-Epsilon Turbulence
Realizable K-Epsilon Two-Layer
Two Layer All Y+ Wall treatment

(b) Phase specific

Oil
Turbulent
Energy
Liquid
User Defined EOS

Air
Turbulent
Energy
Gas
Ideal Gas

The oil is initiated 40 mm below the lower shaft midpoint, without oil in the gear teeth, see figure 35. This is because there is very little oil between the gear teeth when the gears are rotating and having oil between them initially increases the needed physical time to reach convergence.

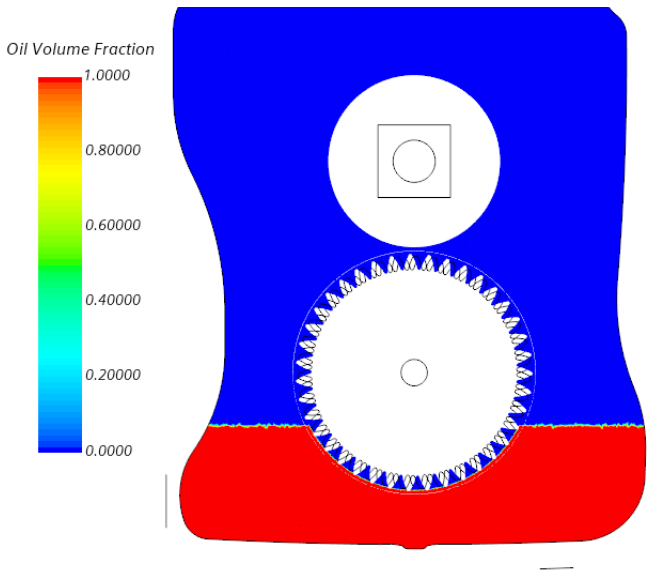

Figure 35: Section view at the middle of the gear showing the initialized oil level

The oil is modeled as a compressible fluid with the definition $\rho = 805.6+P/2134521$ where P is pressure in Pascal. The temperature in the simulation was constant at 80 ° C and the corresponding dynamic viscosity used in the simulation is 0.01336 Pa·s. Other oil data are the Specific heat, the speed of sound and the thermal conductivity which was 2293.62 J/(kg·K), 1461.0 m/s and 0.135561 W/(m·K) respectively.

8 Results

In this section the major results of the study are presented. These include the estimated standard uncertainty and design verification CFD simulation results.

8.1 Estimated uncertainty and total power loss

The main benefits of the new rig compared to the existing Volvo one is the much lower estimated uncertainty. The estimated uncertainty of the chosen concepts, at 1200 RPM are presented in table 7. The data are a combination of test results and data from SKF [23] as described earlier in section 4.1.3.

Table 7: Component losses and uncertainties at 1200 RPM

Component	Loss		Uncertainty	
	[mN·m]	Watts	[mN·m]	Watts
Main shaft bearings (SKF 61804. SKF 61806)	33.74	0.95	0.41	0.052
Lower shaft bearings (SKF 61900. SKF 61800)	1.97	0.25	0.04	0.005
Kistler torque sensor (4503A20L00B1CD1)	0	0	0.16	0.020
Radial gap seal (1 mm gap)	0.20	0.025	0.05	0.006

The total uncertainty was calculated using equation 1 and equation 2 in chapter 2.6 to 0.079 W with a confidence interval of 95%. This includes the torque sensor, all bearings and the shaft seal but not any uncertainty due to the oil level or test objects which are major parts in the repeatably and reproducibility uncertainties.

The combined power losses from all components, in the designed rig were estimated from tests, calculations and available manufacturer data as 1.223 W at 1200 RPM $\pm$ the uncertainty.

8.2 Simulation Results

In this section the results for the simulation setups described in table 3 are presented. The results are shown in forms of torque, vector and streamline plots. In total, three simulations where run. Each simulation has simulated 2 ± 0.1 s of physical time. The combined cost for this was 200000 core hours.

8.2.1 Common flow characteristics

The flow is unsteady. Figure 36 is a plot of the torque on the lower gear over time. It shows a transient behaviour initiated at the start that is dampened over time. This behaviour is likely because of the sloshing effect which has not fully died out. The measurements can be verified through testing in the test rig, once built. Figure 37 show an overview of the oil distribution in the box for different volume fractions of oil.

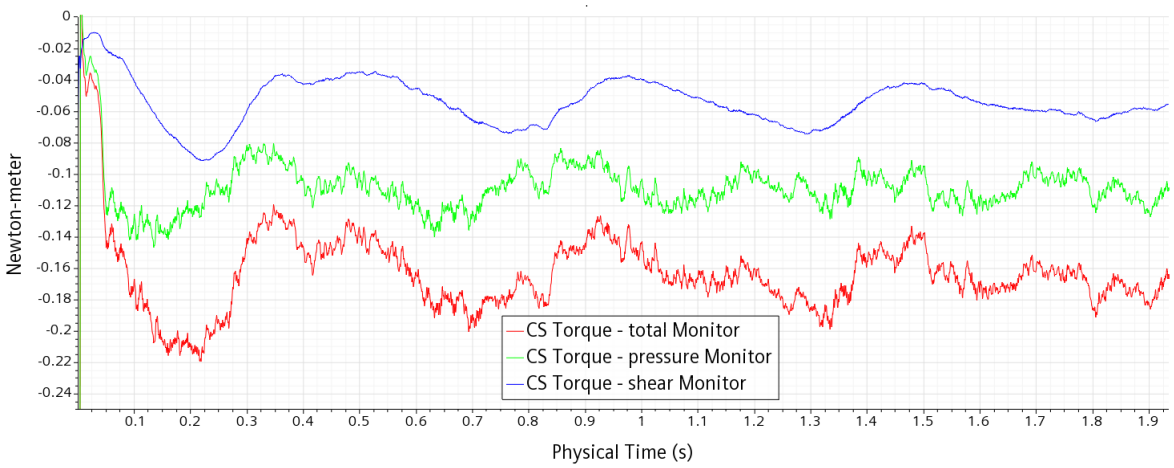

Figure 36: Torque on the lower gear over time due to shear and pressure forces

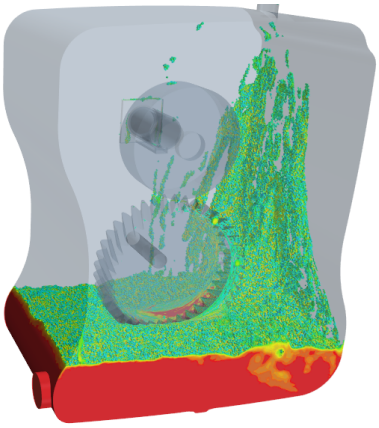

(a) Volume fraction 0.5-1

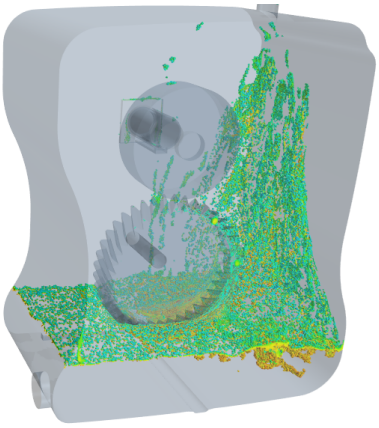

(b) Volume fraction 0.5-0.8

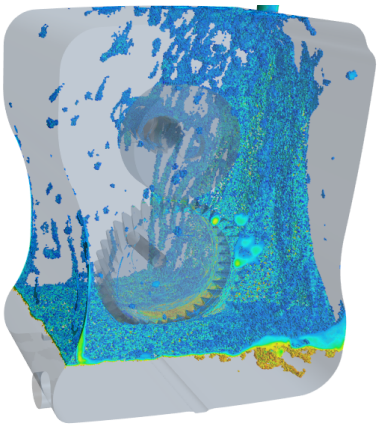

(c) Volume fraction 0.1-0.8

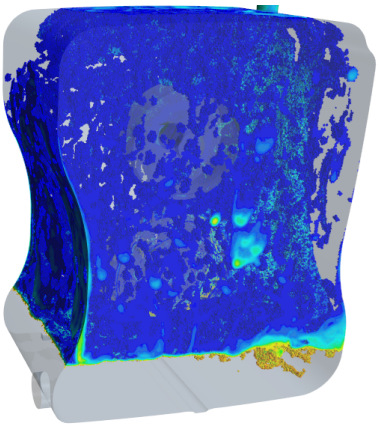

(d) Volume fraction 0.01-0.8

(e) Volume fraction color bar for 37d-37a

Figure 37: Distribution of oil spray in different volume fraction ranges

8.2.2 Oil distribution and mixing

To show the effects of the outlet and inlet on the flows, two velocity line plots are presented. One top down at 105 mm below the lower shaft center and one from the front centered at the hole in the bottom surface, see figure 38 and figure 39. For easier comparison the color bars have the same scale between both figures.

In figure 38b and 38c there is a vortex present in the top right corner. This vortex is not present in the simulation without in and outflow, see figure 38a. The flow in this area is very complex, which can be seen in figure 39, as there is oil and air splashing into the area from above. The air is visible as white here, since the velocity is only displayed where the volume fraction of oil is ≥ 0.5.

The left side of the domain in figure 38, where the fluid velocity is low, is experiencing a significant change of direction due to the inflow and outflow.

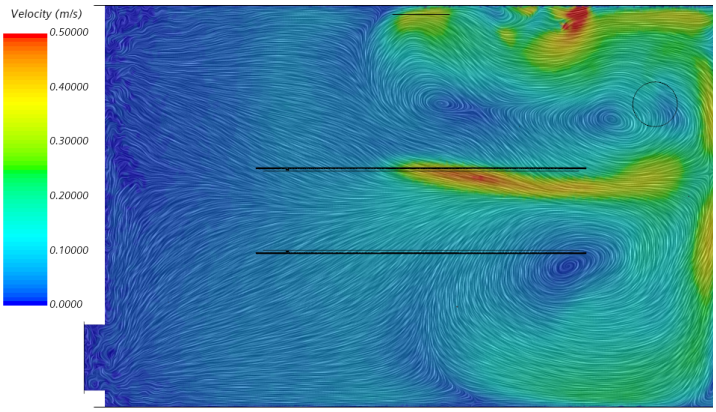

(a) No inlet or outlet flow

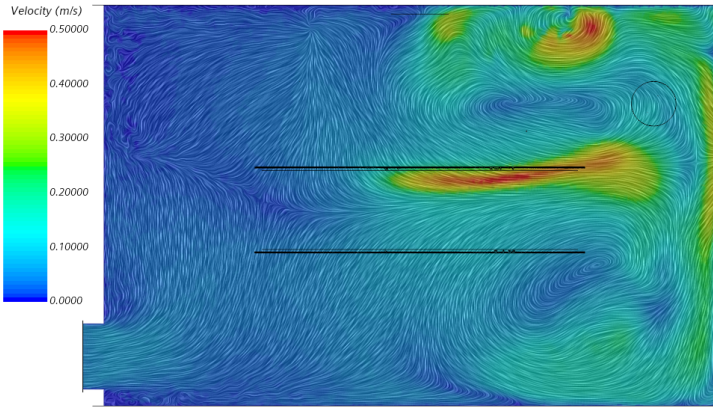

(b) Side inlet and bottom outlet

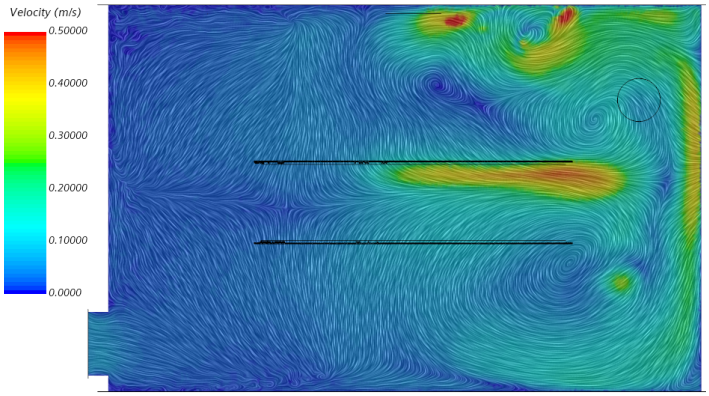

(c) Bottom inlet and side outlet

Figure 38: Velocity lines in a plane 6 cm below the center of the lower shaft

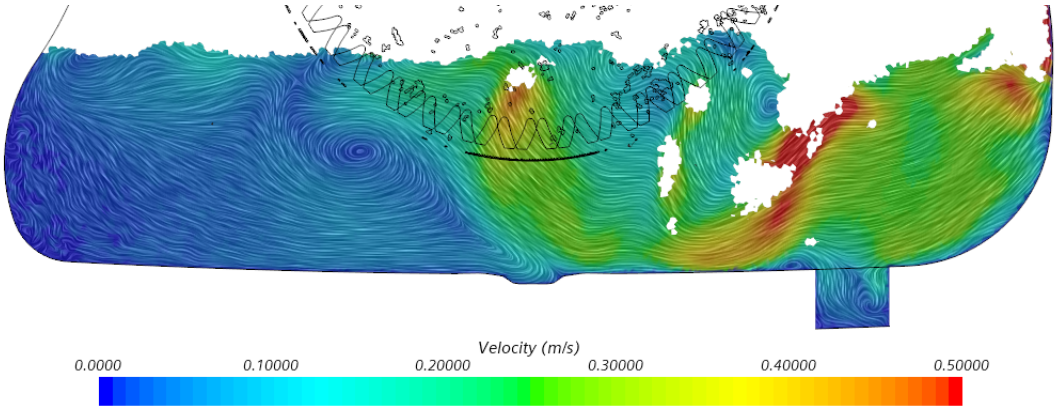

(a) No inlet or outlet flow

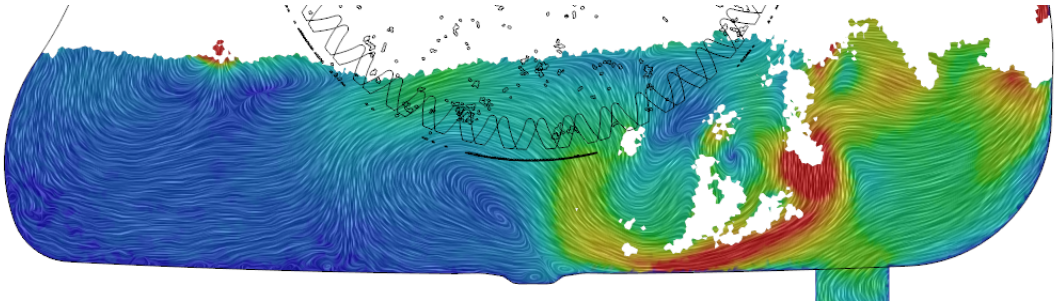

(b) Side inlet and bottom outlet

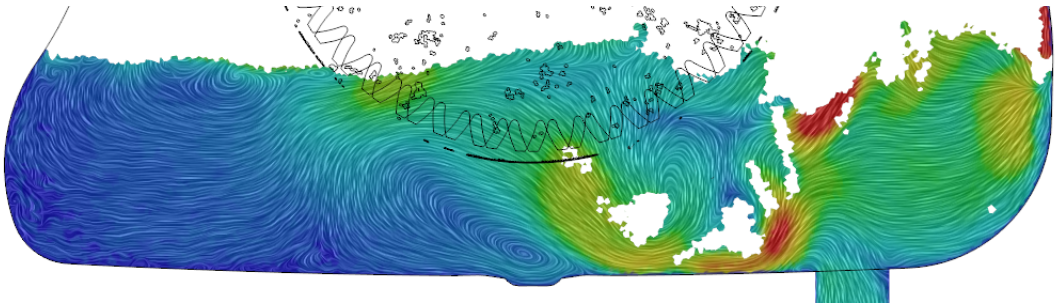

(c) Bottom inlet and side outlet

Figure 39: Velocity lines for volume fraction of oil ≥ 0.5 in a plane centered on the hole at the bottom. Scale of the color map is the same for all sub figures.

Figure 40 shows streamlines originating from the inlet, at the bottom left, and outlet, at the top right. One key aspect of the flow is that there seems to be no shortcuts from inlet to outlet, meaning the oil will mix in the bulk fluid before it goes from inlet to outlet.

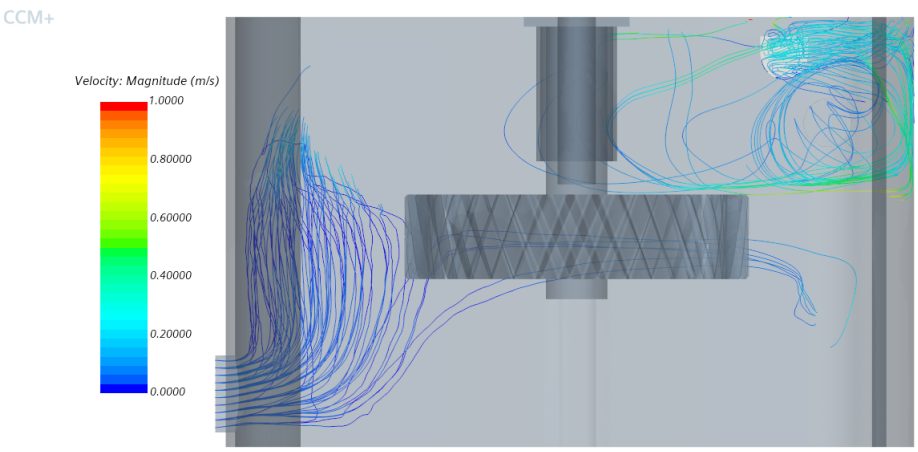

Figure 40: Top down view of streamlines emanating from the inlet on the left and outlet on the top right, lines cut of when they reach an oil volume fraction less than 50%

8.2.3 Predicted seal efficiency

. Figure 41 shows how far the oil penetrates into the upper shaft seal and the volume fraction of that oil. The oil enters the shield near the gear, left in the figure. It is rapidly thrown out from the shaft onto the inside of the shield. The oil remains on the shield inside surface until it flows out through the protected hole in the bottom of the shield. A small amount of oil reaches the end of the shield, right side in the figure, where it meets an edge. This edge stops the oil from progressing further axially. The volume fraction of oil at this point is less than 5% in all cells.

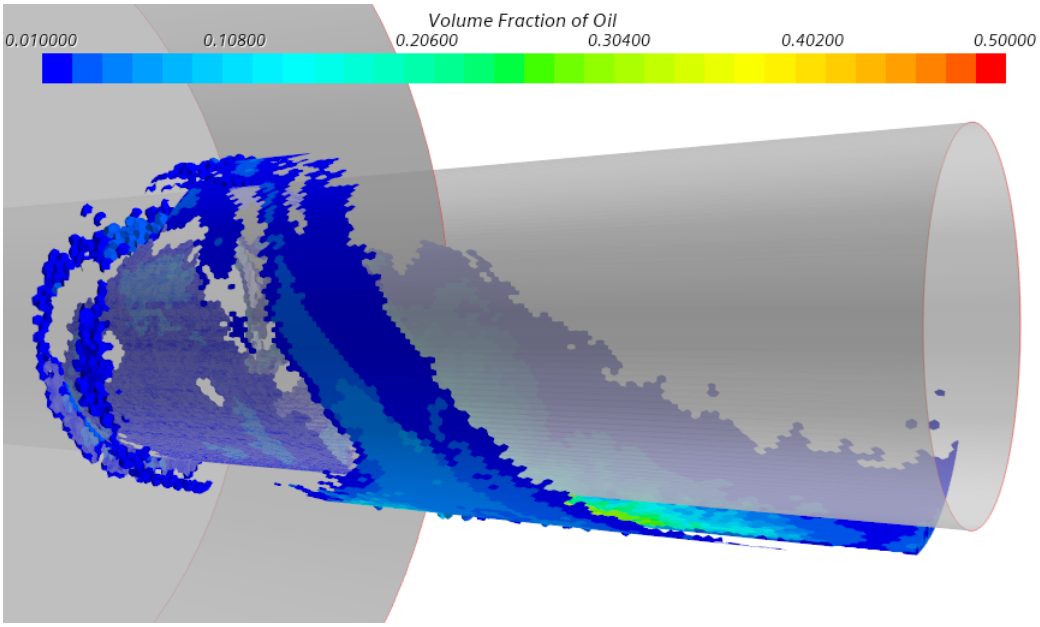

Figure 41: Section view at the middle of the gear showing the initialized oil level

9 Discussion

The rig is able to accommodate and measure torque on one gear running at speeds up to 3000 RPM, and, the rig is able to support two shafts with one gear on each shaft. This has been validated through hand calculations and FEA simulations on the shafts, both static and dynamic, see section 4.2. The engine and torque sensor where selected before the study and have proven able to accommodate the demands in previous tests conducted at Chalmers [9] [10] [11] [30] [31]. The selected bearings are rated for speeds below 80000 RPM according to the manufacturer [23], which is well above the requirement.

The oil level is able to be measured to within $\pm$ 1 mm with the sight glass. A visual inspection on the flow in the axial direction from both sides is possible. The current design requires presence at the rig if continuous oil level measurements is required. Operation of the rig itself is possible to do from a remote location limited by cable length limitations.

Tests are possible to be run at the installation shaft angle on flat ground, 4° incline and the incline angle can deviate more than $\pm 11.3°$ from this angle. This is due to the implementation of a tilt system which is discussed in section 5.2.3.

The design indicate that it is possible to fill/empty the bulk oil in a matter of minutes. To limit the residual oil in the box a sloped surface at the back of the box funnels the oil towards the outlet. Furthermore, the design indicate that an operator can change test objects in much less than 2 hours as it only requires the latching an unlatching of four latches and the removal and replacement of four screws. There is a risk of delay if the parts need to be dried of oil. If this is a necessity can easily be determined through physical tests of the rig. Finally running tests with an oil gutter or similar modifications is possible as the box is large enough and has threaded holes on the sides for fastening of these kinds of additions.

The rig is able reproduce the range of viscosity the 97307 transmission oil has between $20°C - 80°C$. This is achieved using different oils in combination with Volvo GTT's oil conditioning system. The box materials are stable at a temperature of up to $80°C$ but the maximum temperature is limited due to safety concerns discussed further in 6.4

CFD simulations indicate that the intended placement of the inlet on the side results in sufficient mixing throughout the box. No apparent shortcuts where the oil goes straight from the inlet to outlet without mixing were observed, see figure 38 in chapter 8.2.2. The inlet and outlet streamlines are separated which is good because oil is only exchanged between them when oil is added or removed from one. The inlet oil seems to be joining the oil flow feeding the gear which results in thorough mixing through churning. This seems to be in line with what was predicted when deciding the placements of the inlet and outlets.

Comparing the box with and without inlets there are differences, but this is expected. Ways to minimize these difference are discussed in the section 11.

The CFD simulations also show that the upper axle shield seems sufficient to keep oil from leaking out at the upper shaft, see section 8.2.3. An additional o-ring preventing oil to run along the shaft when the rig is stopped will be fitted in the real box. If this is later discovered to not be sufficient, modifications to the part is possible and easily implemented as the part is well suited

for 3D-printing.

The CFL number was chosen to interface and the mean general flow in the box and not at the gear teeth as the distribution and mean flow was more interesting than accurately resolve the flow at the gear teeth.

For the lower shaft bearing and the radial gap the loss and uncertainty data is based on calculations and provided by manufactures. The standard uncertainty for these components is calculated assuming that the deviation is normally distributed. To account for possible anomalies, it was assumed that the maximum and minimum values covers 95% of all measurements when transferring manufacture data to standard uncertainty numbers.

The rules for determining the standard deviation of samples was used for calculating the standard uncertainty of the test data. This applies for the data gathered and used for the main shaft bearings, torque sensor and rubber contact seal found in table 2.

10 Conclusion

This study has evaluated and compared possible solutions and components that can be used when designing test rigs for measuring losses in gears with high precision or other test rigs of similar nature and scale.

The estimated test rig uncertainty approximations suggest that the goal of the study: Design a gear test rig with less than 55 W total uncertainty at 1200 RPM, is fulfilled. The calculated total uncertainty is 0.079 W at 1200 RPM which is well below the uncertainty goal. This does, however, only include mechanical components and components estimable from hand calculation. Thus, it does not include uncertainty due to effects from the oil level or test objects, which are major parts in the repeatably and reproducibility uncertainties as mentioned in section 8.1.

A large contributor for successfully improving the torque measurements, as compared to Volvo GTT's test rig, is the inherent simplicity of the design. When testing two different gear parings in Volvo's rig, the entire gearbox must be disassembled and reassembled. In this rig, however, to do the same test one only needs to open the hatch, unscrew the gears and screw on the new gears. This allows for much lower uncertainties between measurements, as touching any components other than the test object itself, leads to the uncertainty of how it affects the results.

11 Future improvements and future work

Further work and physic test are needed to verify the function of the gear test rig. These can include repeatability and reproducibility test in the rig with oil. Testing the effects different test object manufacturing methods such as machining, FDM and SLS printing have on the uncertainty.

If the rig needs an even lower uncertainty the upper bearings can be replaced by Air bearings or shaft integrated torque sensors can be implemented in the rig. If the need for digitally read the oil level the level measuring glass can be exchanged for a pressure sensor of the type mentioned in section 5.2.2.

Inlet and outlet flows can also be modified if they are shown to be insufficient through 3D printing channels in the inner profiles. The modification can be made to distribute the oil differently or decrease the inlet and outlet velocity.

References

[1] I-shift transmission. [Online]. Available: https://www.volvotrucks.us/trucks/powertrain/i-shift-transmission/

[2] Kenneth Holmberg and Peter Andersson and Nils-Olof NylundKari Mäkelä and Ali Erdemir, "Global energy consumption due to friction in trucks and buses," *Tribology International*, 2014.

[3] Climate strategy. [Online]. Available: https://www.volvogroup.com/en/sustainability/climate-goals-strategy.html

[4] O. Lygner, "Parameter study of load independent power losses for AT2612F is measured to identify possible pathways to reduce CO2 emissions that originates from amt transmission system." *ER-675797*, 2007.

[5] B.-R. Hoehn, P. Oster, T. Tobie, and K. Michaelis, "Test methods for gear lubricants," *Maziva 2008;47(2):141–52.*, 2008.

[6] International Organization for Standardization, "Gears - fzg test procedures - part 1: Fzg test method a/8,3/90 for relative scuffing load-carrying capacity of oils," *ISO 14635-1*, 2000.

[7] ——, "Gears - fzg test procedures - part 2: Fzg step load test a10/16, 6r/120 for relative scuffing load-carrying capacity of high ep oils," *ISO 14635-2:2004*, 2004.

[8] ——, "Gears - fzg test procedures - part 3: Fzg test method a/2,8/50 for relative scuffing load-carrying capacity and wear characteristics of semifluid gear greases," *ISO 14635-3:2005*, 2005.

[9] E. A. Hartono, A. Pavlenko, and V. Chernoray, "Stereo-piv study of oil flow inside a model gearbox," *17th Lisbon International Symposium On Applications of Laser Techniques to Fluid Mechanics*, 2014.

[10] E. A. Hartono, "Piv study of fluid flow inside a gearbox," *PIV13; 10th International Symposium on Particle Image Velocimetry, Delft, The Netherlands*, 2013.

[11] ——, "Study of fluid flow inside the gearbox," *Licentiate thesis*, 2014.

[12] J. Polly, D. Talbot, A. Kahraman, A. Singh, and H. Xu, "An experimental investigation of churning power losses of a gearbox," *J. Tribol.*, 2018.

[13] J.-B. Boni, C. Changenet, and F. Ville, "A model for predicting churning losses in planetary gears," *Power Transmission Engineering*, 2019.

[14] P. M.T.Marques, C. M.C.G.Fernandes, R. C. Martins, and J. H. Seabra, "Power losses at low speed in a gear box lubricated with wind turbine gear oils with special focus on churning losses," *J. Tribol.*, 2013.

[15] P. M. T. Marques, C. M. C. G. Fernandes, R. C. Martins, and J. H. O. Seabra, "Power losses at low speed in a gearbox lubricated with wind turbine gear oils with special focus on churning losses," *Tribology International*, 2013.

[16] C. H. Simmons, D. E. Maguire, and N. Phelps, *Manual of Engineering Drawing*. Butterworth-Heinemann, 2020.

[17] X. Zhou, P. D. Walker, and N. Zhang, "Study of power losses in a two-speed dual clutch transmission," *ResearchGate*, 2014.

[18] H. Lundh, *Grundläggande hållfasthetslära*. Instant Book AB, Stockholm, 2000.

[19] O. Matsushita, M. Tanaka, H. Kanki, M. Kobayashi, and P. Keogh, *Vibrations of Rotating Machinery*. Springer, Tokyo, 2017.

[20] H. K. Versteeg and W. Malalasekera, *An Introduction to Computational Fluid Dynamics*. Pearson Education Limited, 2007.

[21] G. Houzeaux, B. Eguzkitza, R. Aubry, H. Owen, and M. Vázquez, "A chimera method for the incompressible navier-stokes equations," *Int. J. Numer. Meth. Fluids 2013; 00:1–45*, 2013.

[22] C. T. Crowe, J. D. Schwarzkopf, M. Sommerfeld, and Y. Tsuji, *Multiphase Flows with Droplets and Particles*. CRC Press, 2012.

[23] SKF, "Rullningslager," BU/P1 17000/1 SV 2019.

[24] "Rotary seals," Trelleborg Group, Edition September 2020.

[25] Arbetsmiljöverket, "Belastningsergonomi, arbetsmiljöverkets föreskrifter och allmänna råd om belastningsergonomi," AFS 2012:2.

[26] H. S. Nliwa, *Handbook of Low and High Dielectric Constant Materials and Their Applications*. Academic Press, 1999.

[27] A. Jacobsson and S. Lamnevik, "Tolerabel risk inom kemikaliehanterande verksamheter, en vägledning från IPS," 2001.

[28] A. R. Moritz and J. F. C. Henriques, "Studies of thermal injury ii. the relative importance of time and surface temperature in the causation of cutaneous burns," *Am J Pathol. 1947 Sep; 23(5): 695–720*, 1946.

[29] N. Imtiaz, "Cfd simulation of dip-lubricated single-stage gearboxes through coupling of multiphase flow and multiple body dynamics, an initial investigation," *Linköpings universitet*, 2018.

[30] M. N. Mastrone, E. A. Hartono, V. Chernoray, and F. Concli, "Oil distribution and churning losses of gearboxes: Experimental and numerical analysis," 2020.

[31] E. A. Hartono, *Experimental Study on Truck Related Power Losses: The Churning Losses in a Transmission Model and Active Flow Control at an A-pillar of Generic Truck Cabin Model*. Chalmers University of Technology, 2019.

A Bearing repeatability data

Rpm	Torque [Nm]	Power [W]
1200	0,032662	4,104641421
1197,60479	0,033116	4,153388931
1197,60479	0,033447	4,194902753
1197,60479	0,034086	4,275045752
1200	0,034446	4,328837131
1197,60479	0,033886	4,249961871
1198,134305	0,033721	4,231137619
1200	0,034052	4,279323056
1197,60479	0,034135	4,281191302
1200	0,034095	4,284726877
1200	0,034161	4,293021113
1200	0,034113	4,286988941
1200	0,034227	4,301315349
1200	0,033555	4,216864946
1197,60479	0,033533	4,205688822
1200	0,033555	4,216864946
1200	0,03338	4,194872654
1198,463095	0,033623	4,219998811
1197,60479	0,033654	4,22086457
1197,60479	0,033415	4,190889332

Table 8: Bearing repeatability data

B Technical drawings

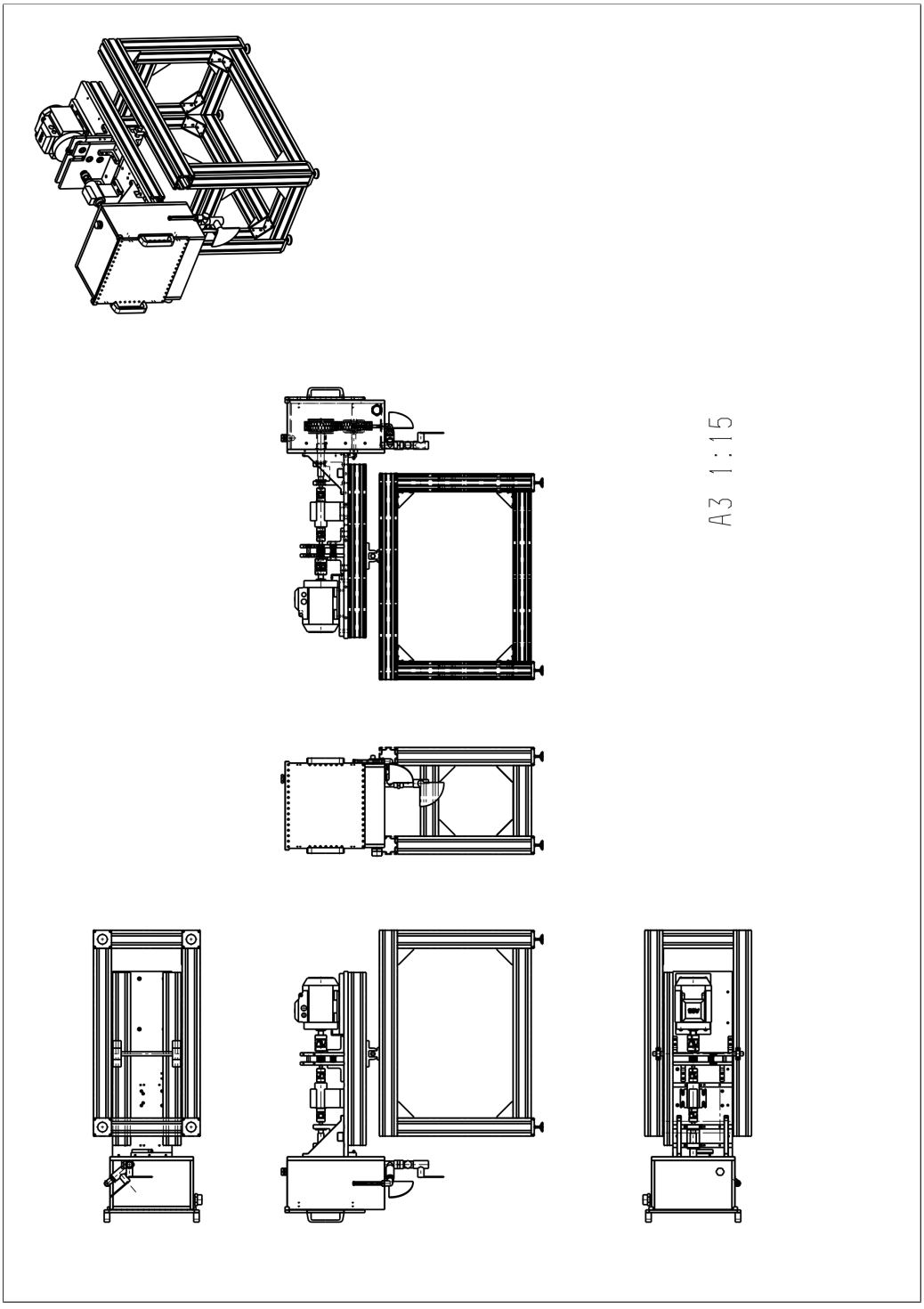

B.1 Box Assembly

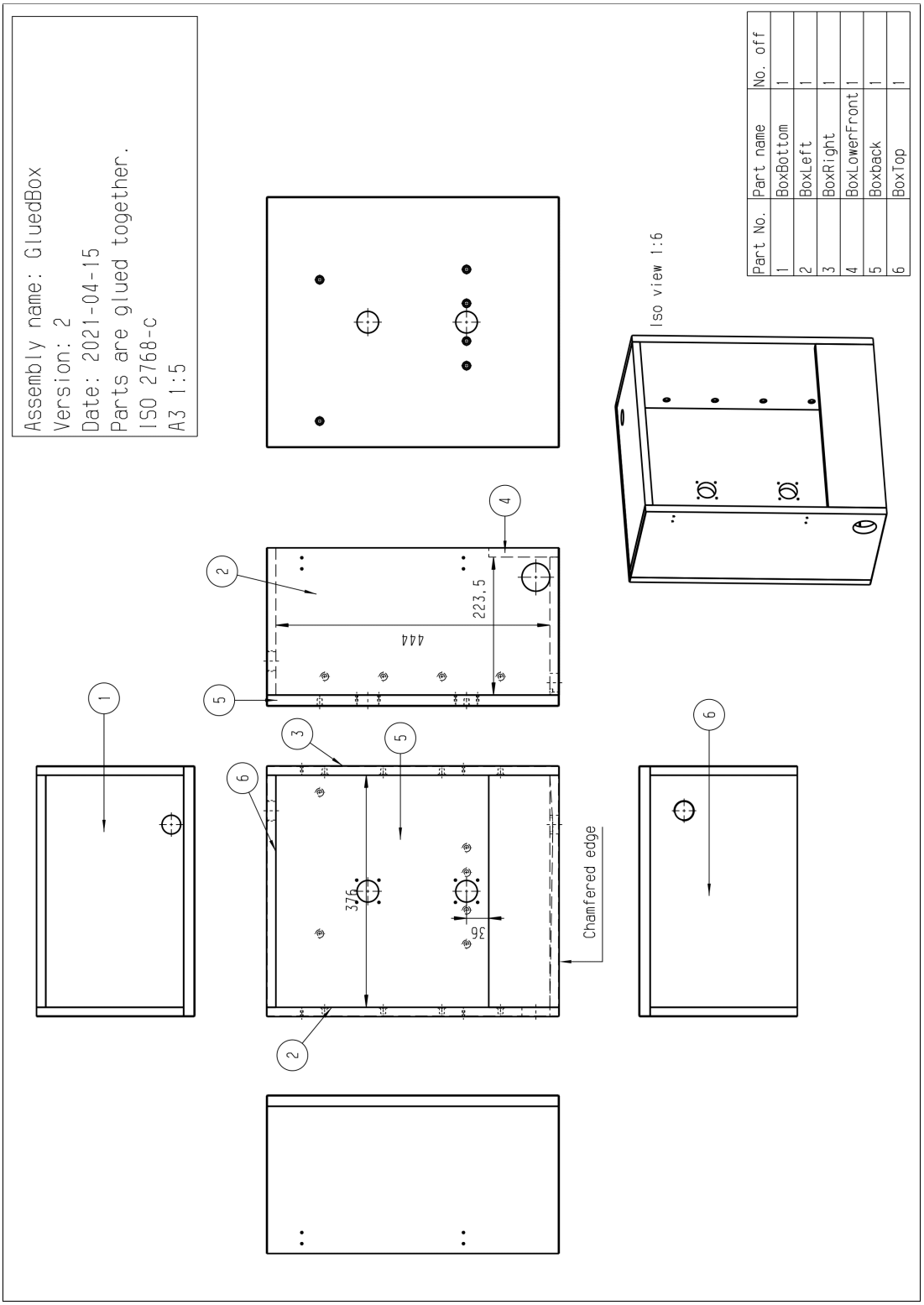

B.1.1 Box Left

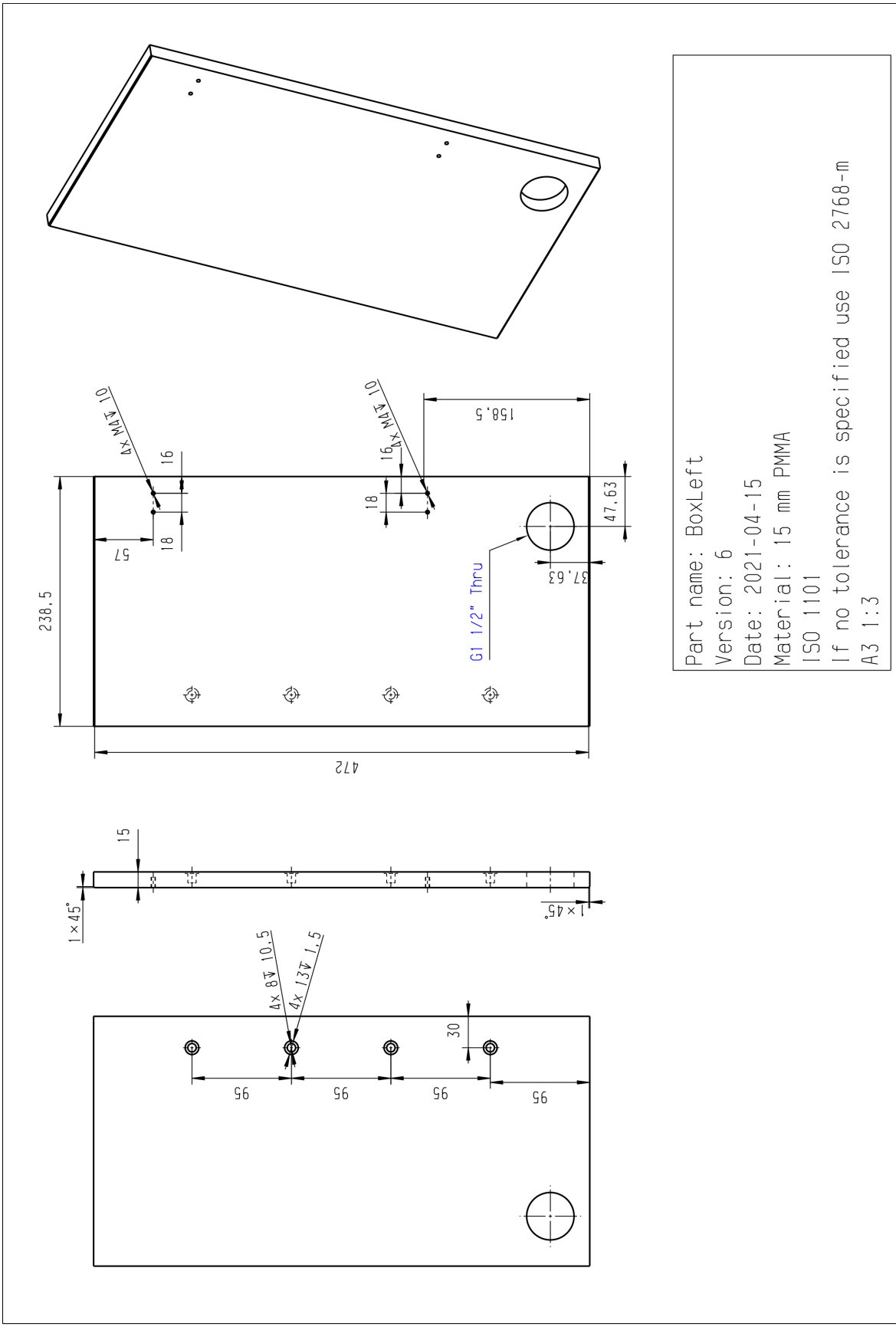
Part name: BoxLeft
Version: 6
Date: 2021-04-15
Material: 15 mm PMMA
ISO 1101
If no tolerance is specified use ISO 2768-m
A3 1:3
4x M4 ↧ 10
16
18
57
4x M4 ↧ 10
16
18
158,5
47,63
37,63
G1 1/2" Thru
238,5
472
15
1×45°
1×45°
4x ⌀8 ↧ 10,5
4x ⌀13 ↧ 1,5
30
95
95
95
95

B.1.2 Box Right

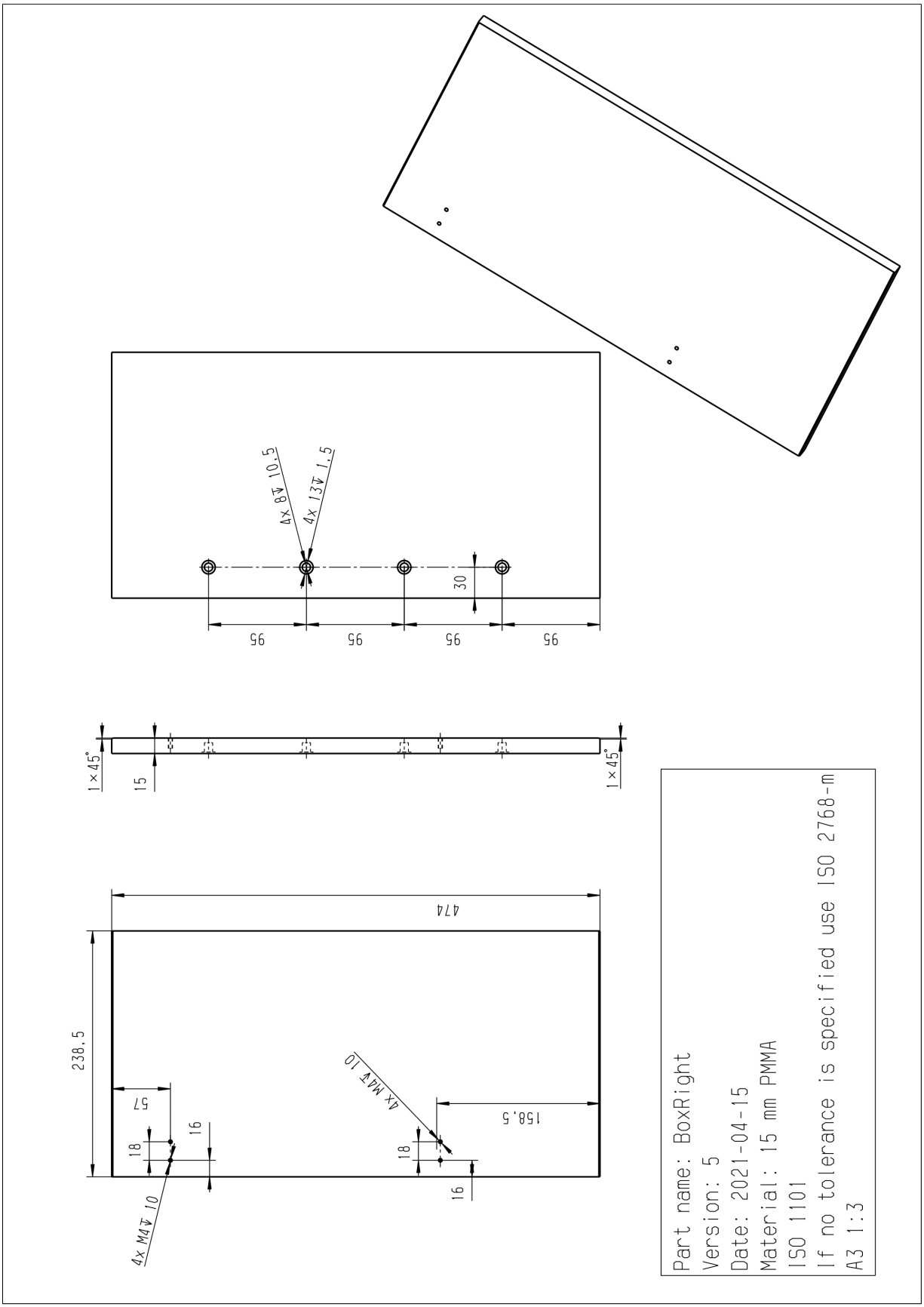

B.1.3 Box Top

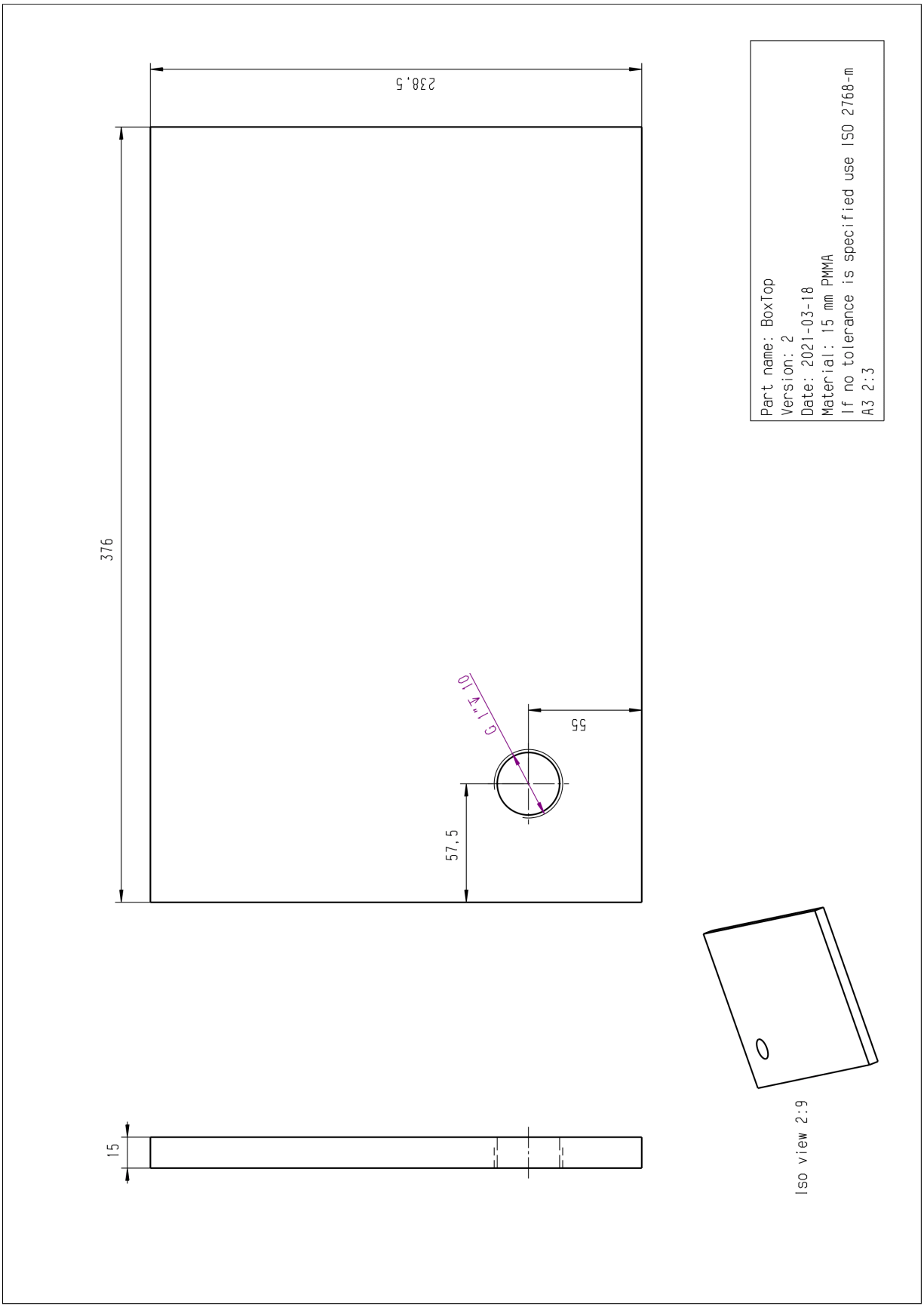
238,5
376
G 1/4"T10
55
57,5
15
Part name: BoxTop
Version: 2
Date: 2021-03-18
Material: 15 mm PMMA
If no tolerance is specified use ISO 2768-m
A3 2:3
Iso view 2:9

B.1.4 Box Bottom

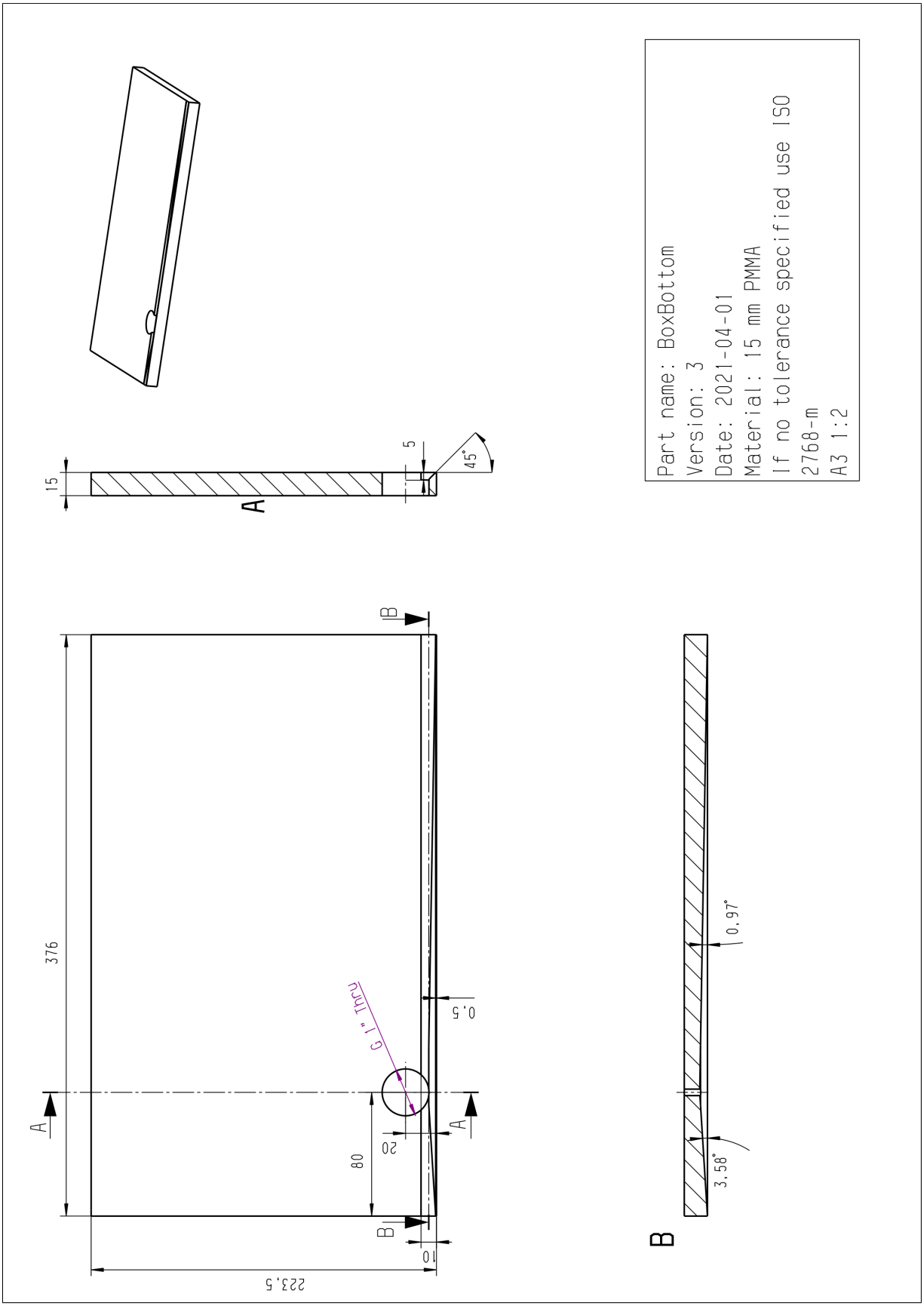

B.1.5 Box Lower Front

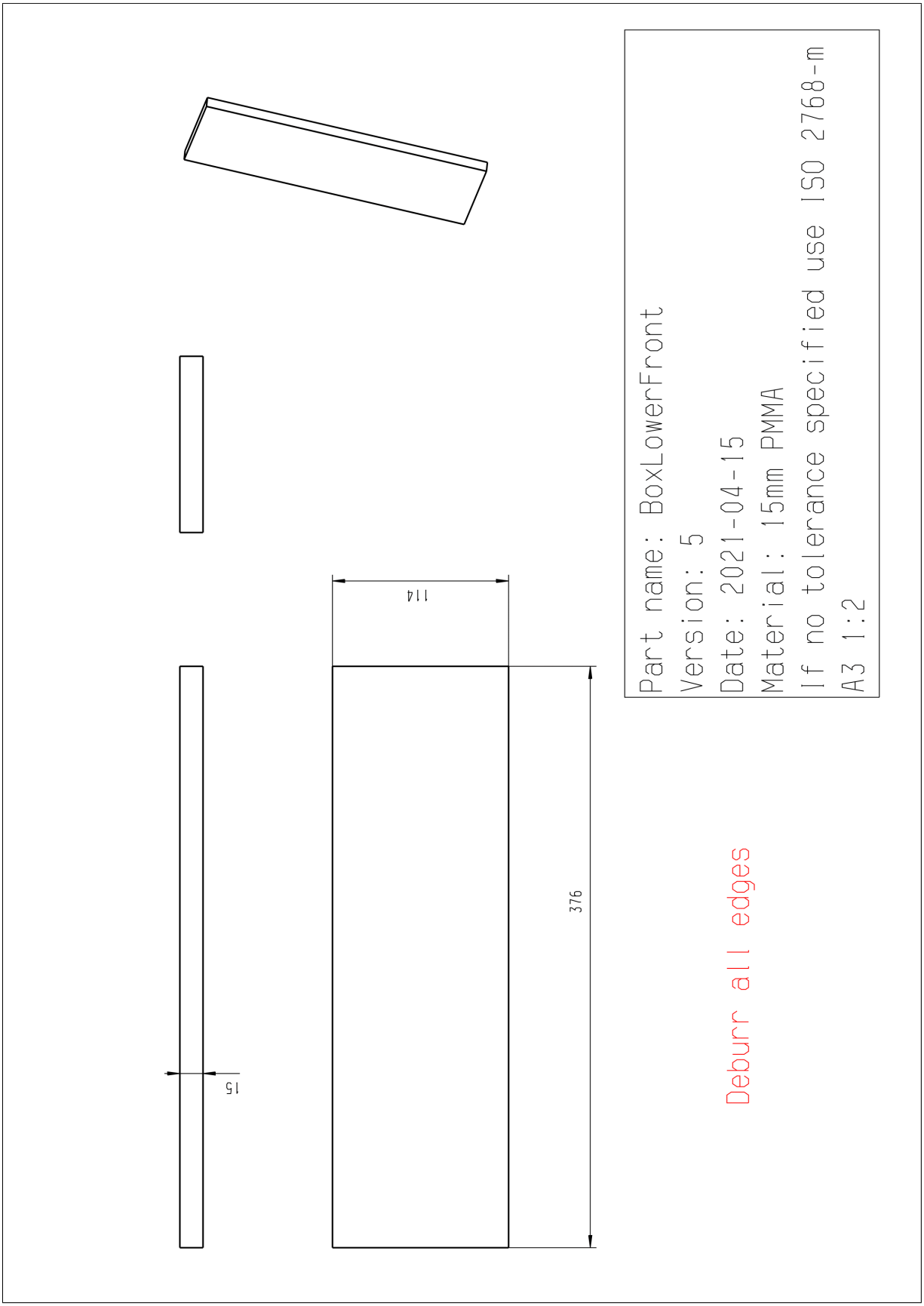

B.1.6 Metal Frame

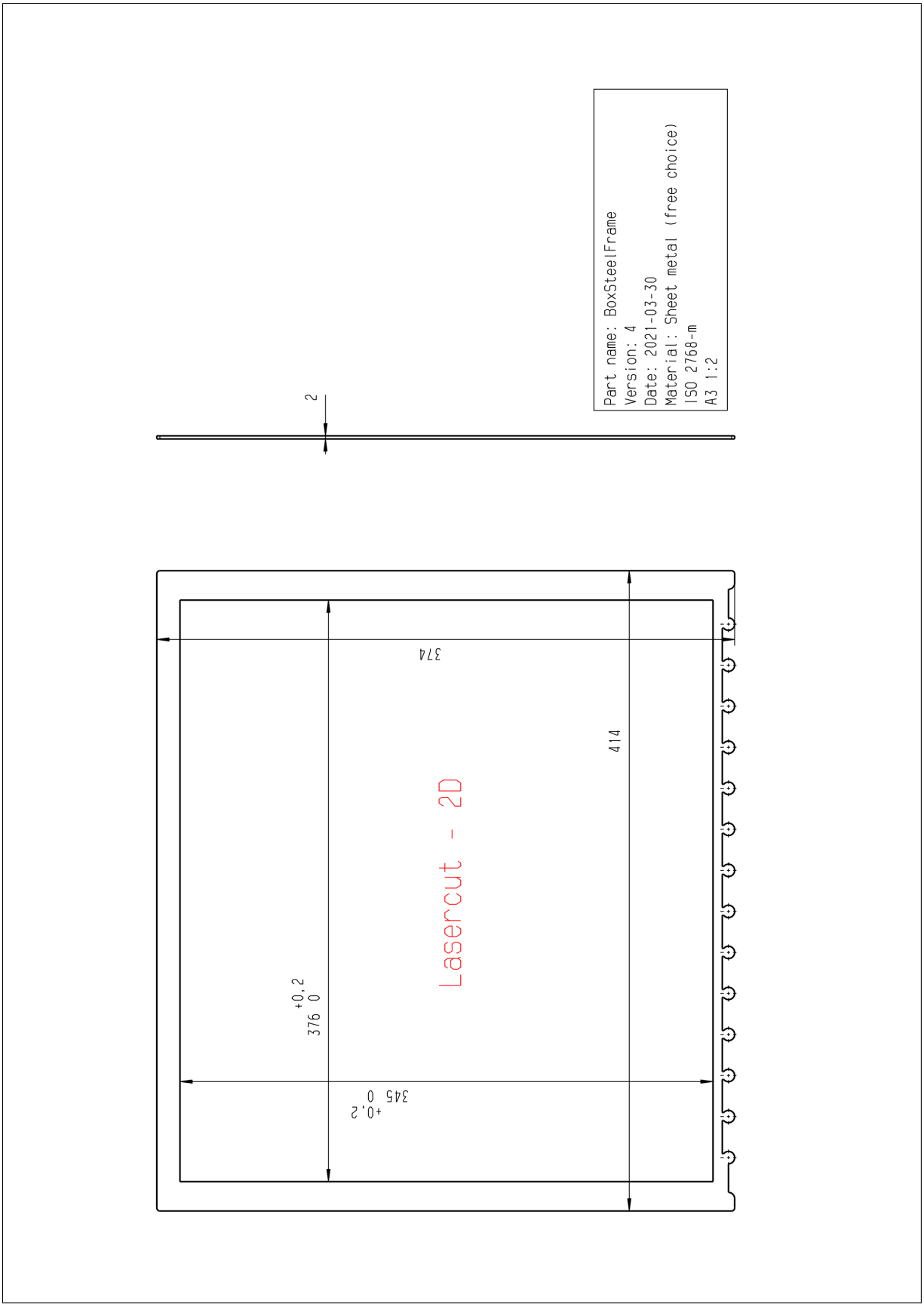

B.1.7 Box Hatch

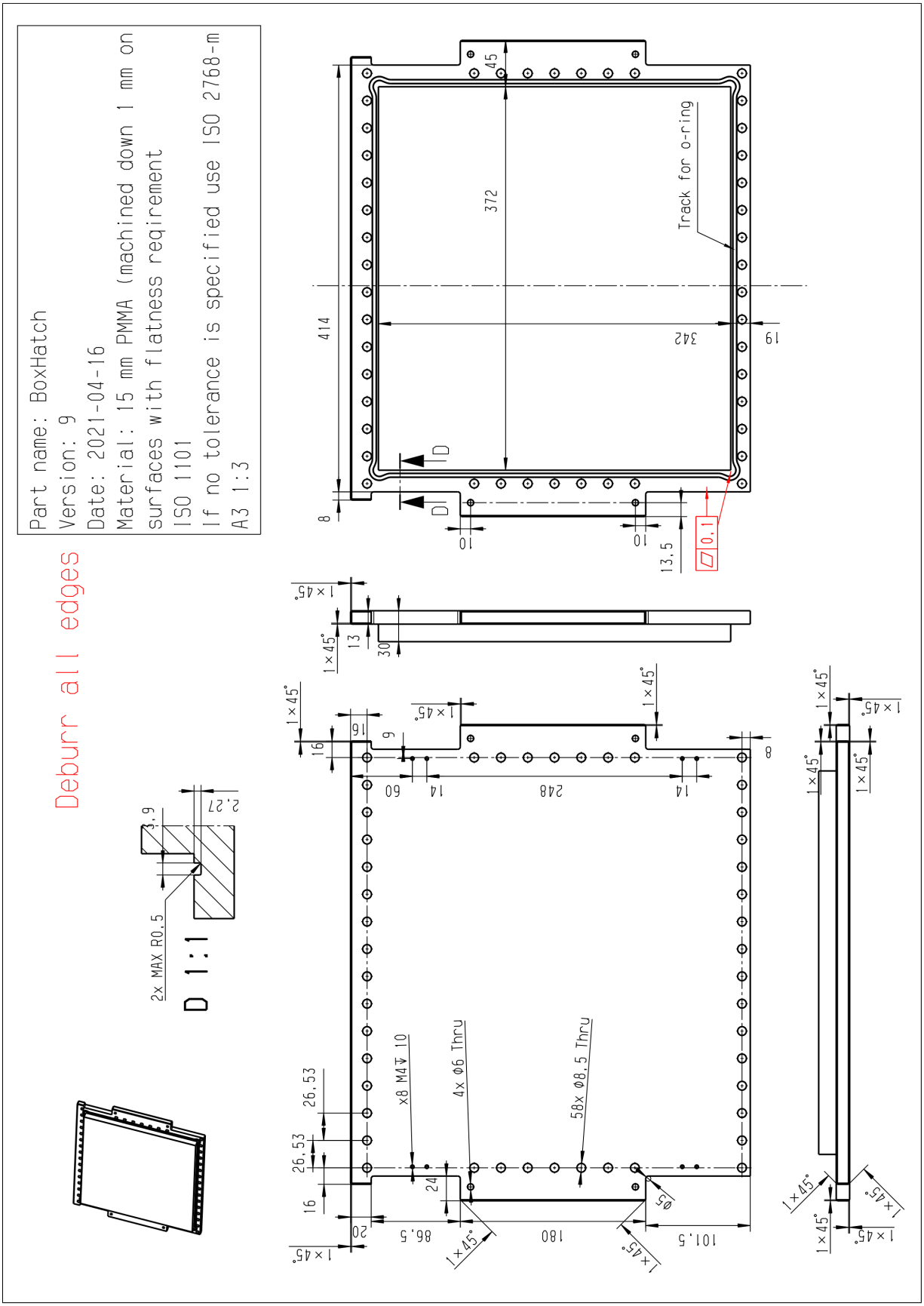

B.1.8 Brace

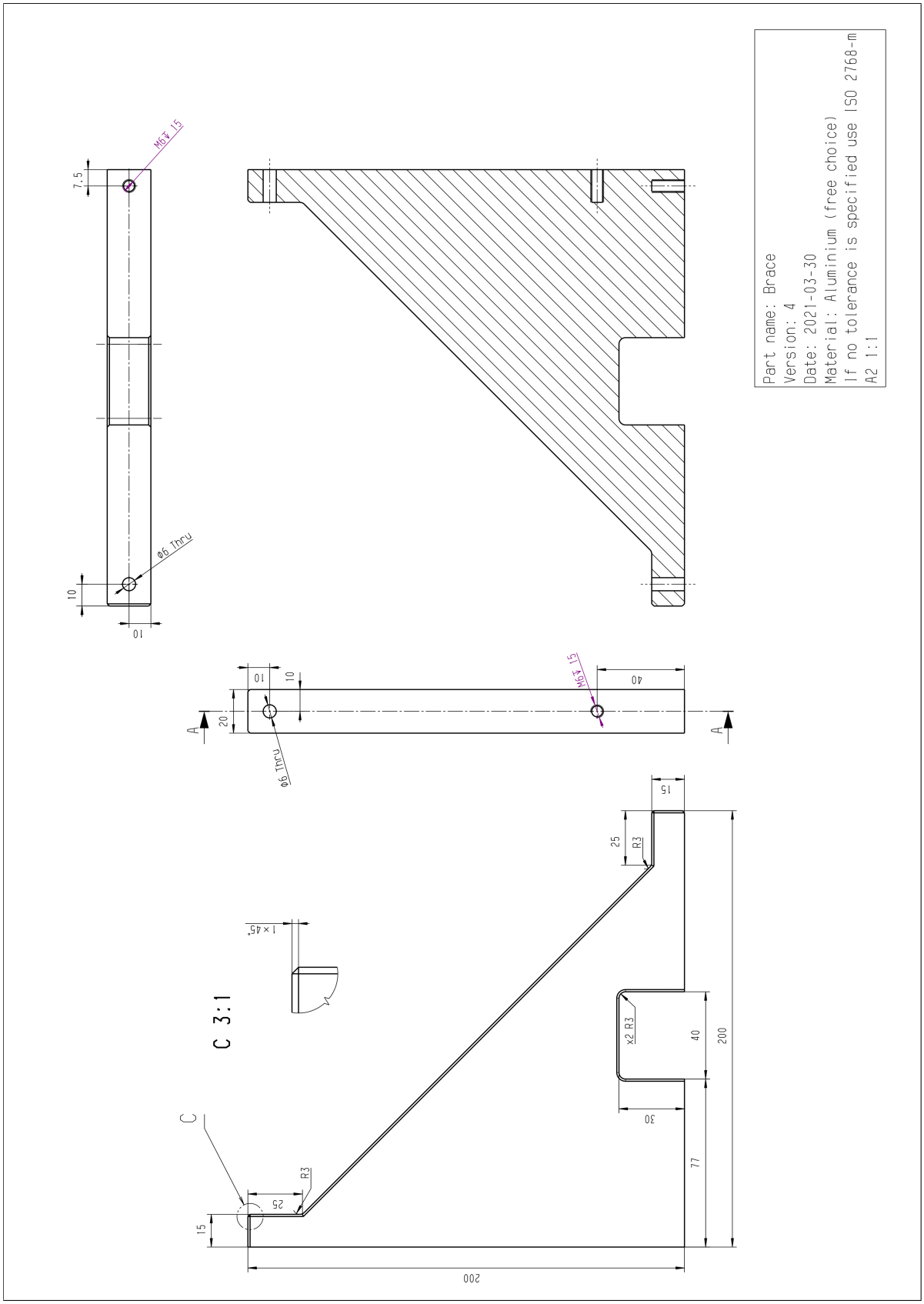
Part name: Brace
Version: 4
Date: 2021-03-30
Material: Aluminium (free choice)
If no tolerance is specified use ISO 2768-m
A2 1:1
M6↧15
7.5
10
Φ6 Thru
10
10
10
20
A
A
M6↧15
40
Φ6 Thru
15
25
R3
1×45°
C 3:1
C
×2 R3
40
200
30
77
R3
25
15
200

B.2 Lower Shaft

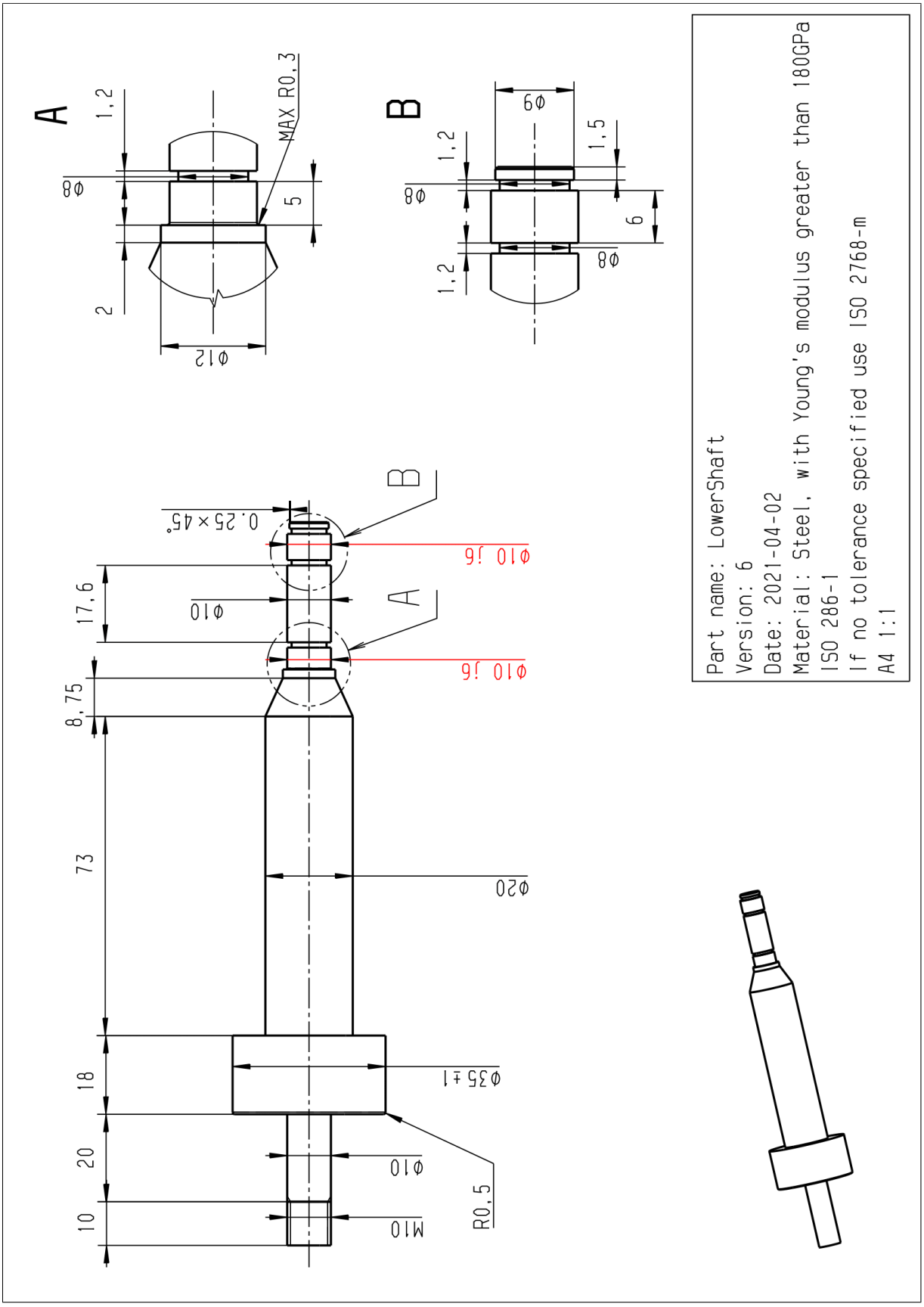

B.3 Upper shaft

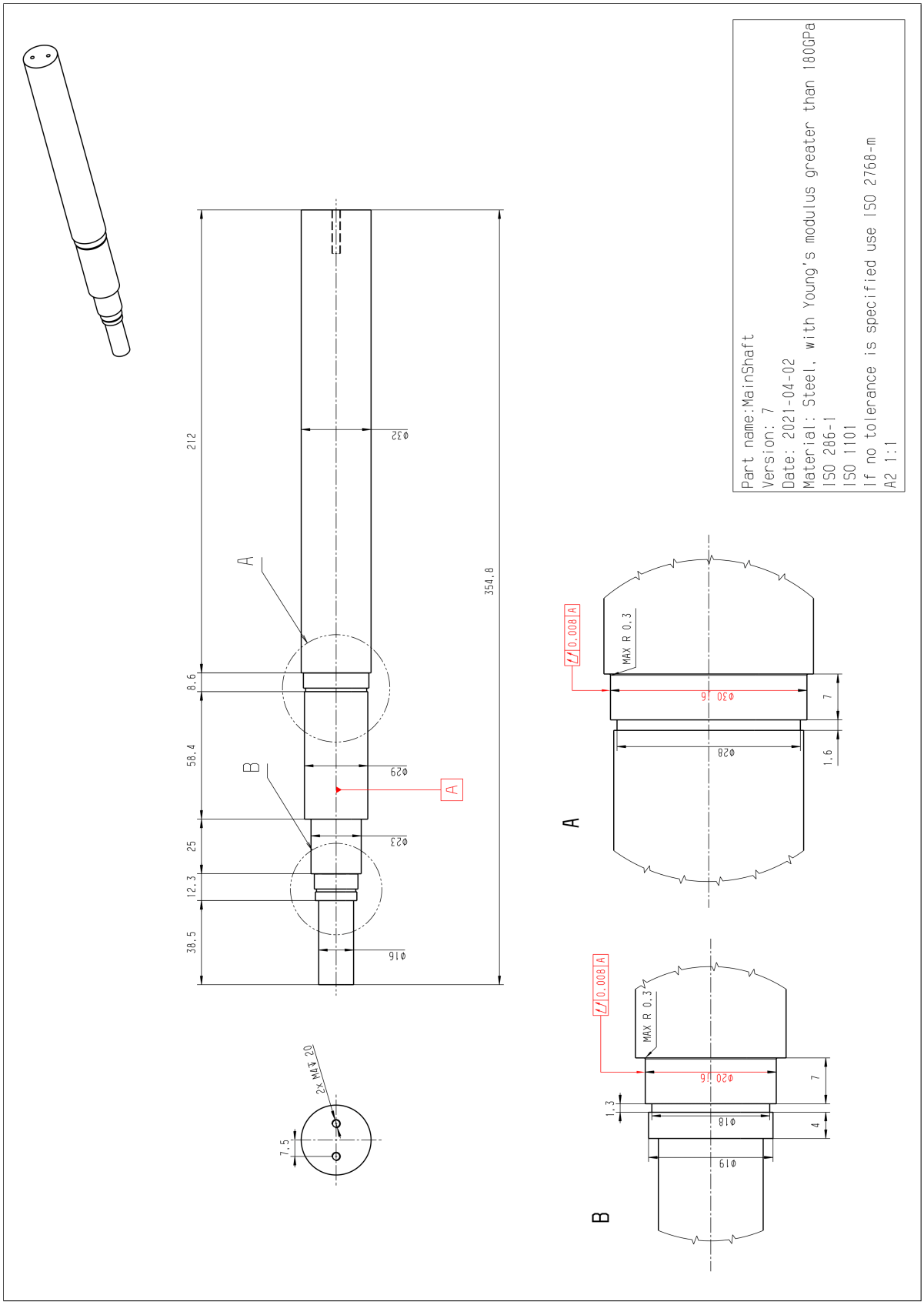

B.4 Lower Gear Fastening

B.4.1 Lower Gear Fastener

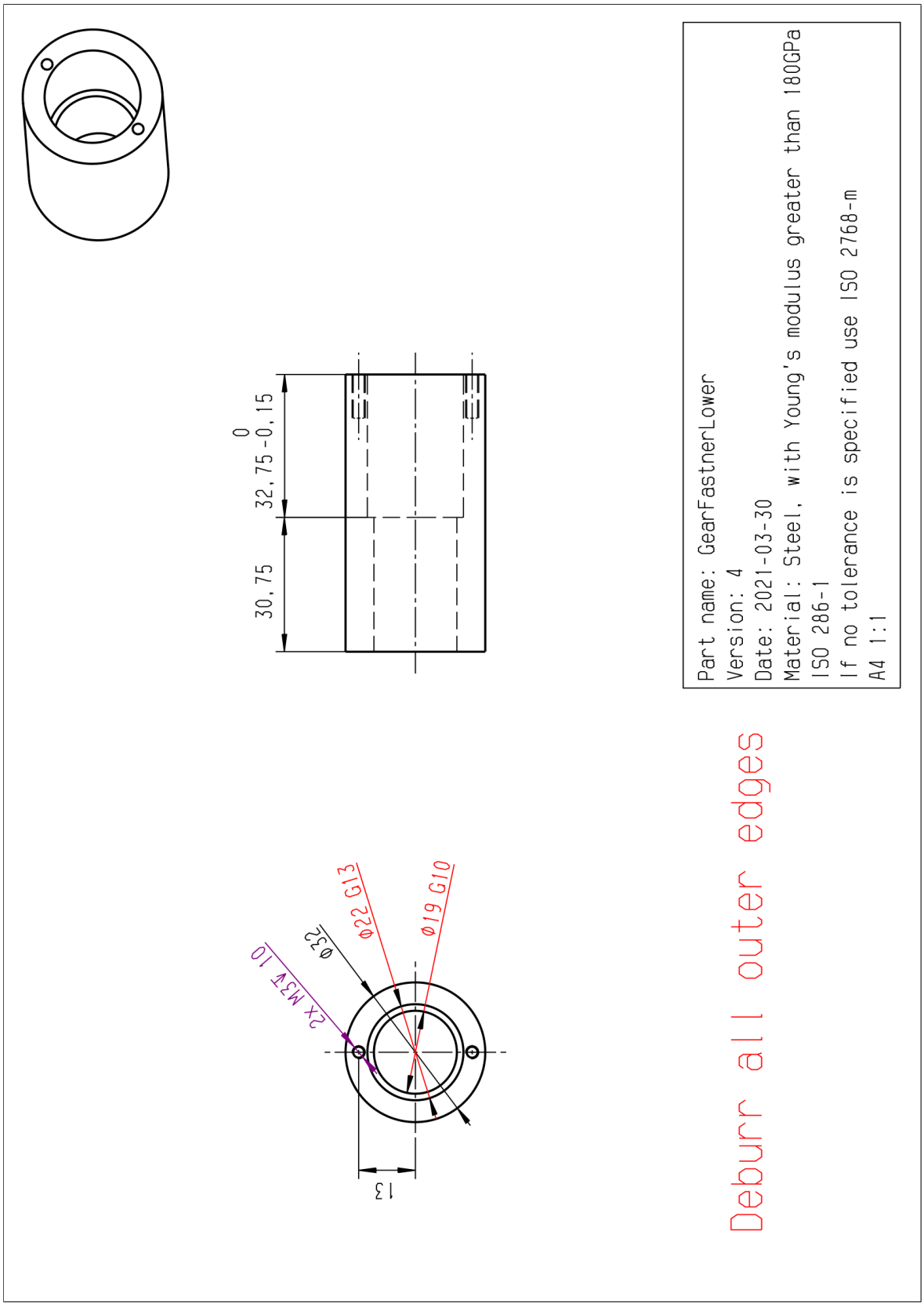

B.4.2 Lower Gear Fastener 2

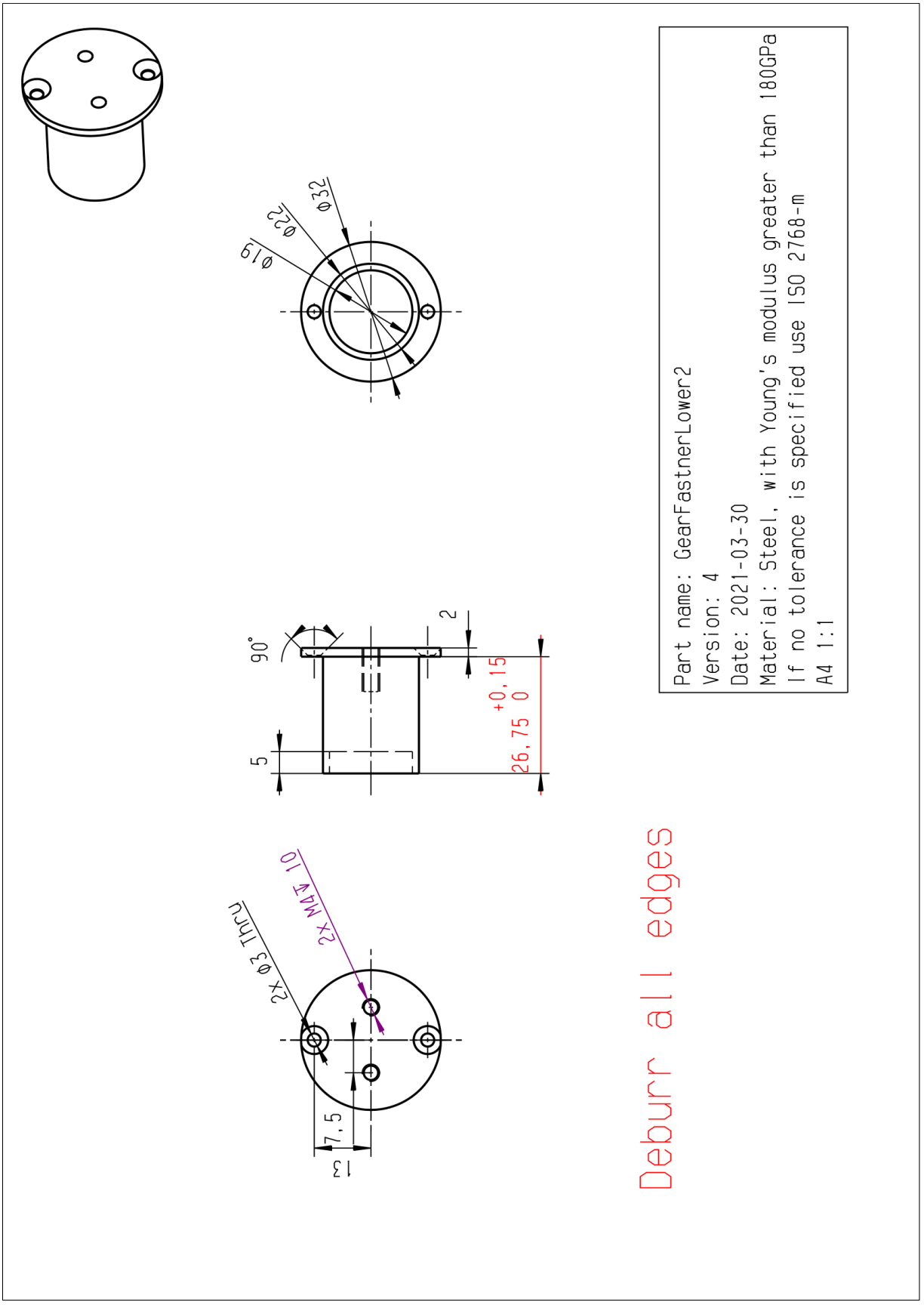

B.5 Bearing Holder

B.5.1 Bearing Holder Replacement

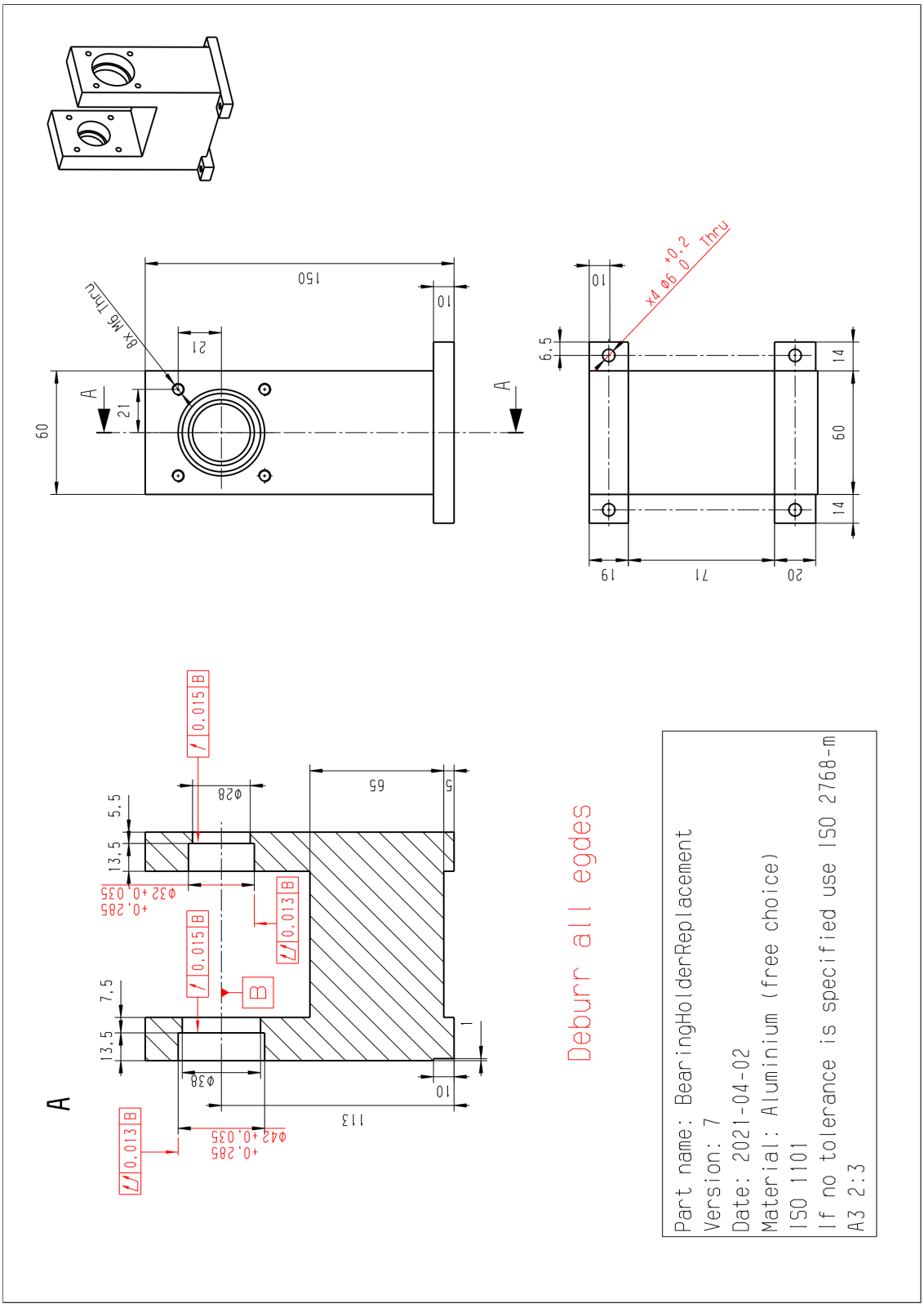

B.5.2 Bearing Holder Replacement 2 large

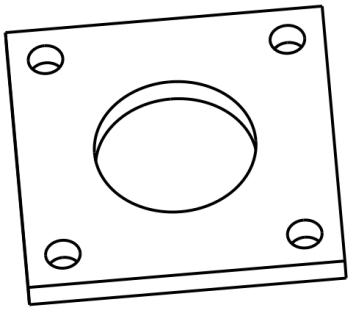

Part name: BearingHolderReplacement2
Version: 5
Date: 2021-04-02
Material: Aluminium (free choice)
If no tolerance is specified use ISO 2768-m
A4 1:1

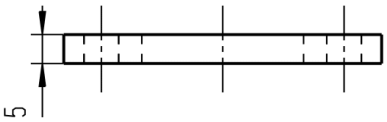

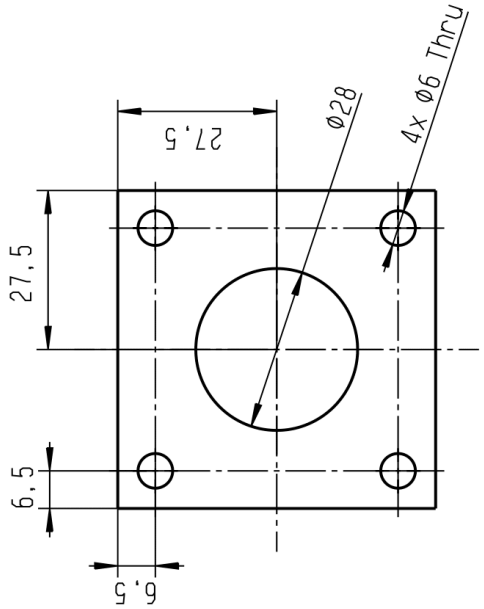

B.5.3 Bearing Holder Replacement 2 small

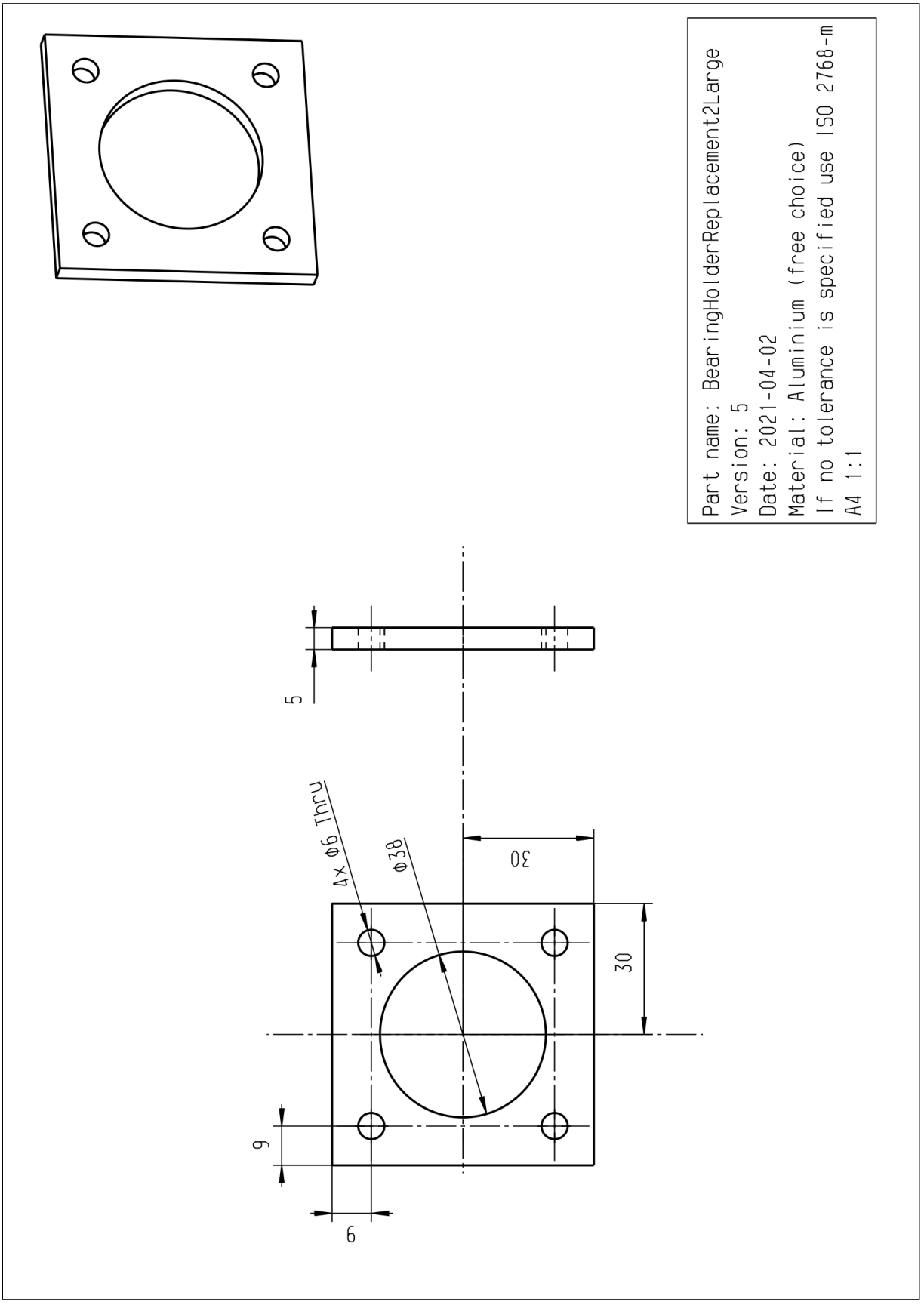

CHALMERS

CHALMERS